



Review

Recent progress of flexible perovskite solar cells

Guanqi Tang, Prof. Feng Yan*

Department of Applied Physics, The Hong Kong Polytechnic University, Hung Hom, Kowloon, Hong Kong



ARTICLE INFO

Article history:

Received 9 October 2020

Received in revised form 6 February 2021

Accepted 4 April 2021

Available online 22 April 2021

Keywords:

Flexible perovskite solar cell

Transparent electrode

Charge transport layer

Low temperature processing

Roll to roll process

ABSTRACT

Perovskite solar cells (PSCs) have been regarded as a promising new generation photovoltaic technology for their high power conversion efficiency, facile fabrication and low cost. Flexible perovskite solar cells (FPSCs) are supposed to be the foremost commercialization option of PSCs because the devices can be prepared by roll-to-roll printing process and suitable for mass production. More importantly, FPSCs prepared on ultrathin and lightweight substrates can meet the demands from the emerging market of flexible electronics and find applications that cannot be achieved with conventional photovoltaic devices. So far, many breakthroughs of FPSCs have been reported and efficiency over 21% has been achieved. In this review, the recent progress of FPSCs is described in details. Many critical issues, including device design, substrates, perovskite materials, electrode materials and charge transport layers, are elucidated and discussed comprehensively. Finally, conclusion and outlook for this field are addressed.

© 2021 Elsevier Ltd. All rights reserved.

Contents

| | |
|----------------------------------------------------------------------------------|----|
| Introduction | 2 |
| Flexible substrates | 4 |
| Flexible glass..... | 4 |
| Metal foils | 4 |
| Polymer substrates | 5 |
| Influence of flexible substrates on mechanical strain in devices | 6 |
| Low temperature processable transparent conductive electrodes | 7 |
| Transparent conductive oxide | 7 |
| Metal nanowires | 7 |
| Metal grids | 9 |
| Carbon-based materials | 9 |
| PEDOT:PSS | 10 |
| Charge transport layers | 10 |
| ZnO | 10 |
| TiO ₂ | 10 |
| SnO ₂ | 11 |
| Other ETLs..... | 13 |
| Hole transport layers | 13 |
| Effect of charge transport layers on the mechanical flexibility of devices | 13 |
| Preparation of high-quality perovskite films on flexible substrates..... | 14 |
| Low-temperature processing methods | 14 |
| Composition and additive engineering | 15 |
| Toward commercialization | 17 |
| Large-area fabrication by R2R method | 17 |
| Device encapsulation | 17 |

* Corresponding author.

E-mail address: apafyan@polyu.edu.hk (F. Yan).

| | |
|-----------------------------------------|----|
| Conclusion and outlook | 21 |
| Declaration of Competing Interest | 21 |
| Acknowledgements | 21 |
| References | 21 |

Introduction

Perovskite solar cells (PSCs) have attracted much attention recently from scientists working on photovoltaic technologies because of the high efficiency, low cost, and solution processability of the devices [1–5]. The highest certified power conversion efficiency (PCE) of PSCs is boosted to 25.5% based on rigid glass substrates due to the intriguing optoelectronic properties of perovskite materials, such as high light absorption coefficient, desirable/tunable bandgap, and long charge diffusion length [6–14]. In addition to the excellent optoelectronic properties, the intrinsic mechanical flexibility and low-temperature solution processability of perovskites make it possible to realize flexible perovskite solar cells (FPSCs) [15,16]. As shown in Fig. 1, FPSCs are expected to find niche applications on unmanned systems [17–19], smart integrated buildings [20], wearable and portable electronics [21,22], and self-powered bioelectronics [23]. More importantly, the fabrication of FPSCs is compatible with roll to roll (R2R) printing process that will enable the mass production and promote the commercialization of perovskite photovoltaic technology in the future. Thus, the development of FPSCs is highly significant for the practical applications of PSCs.

In 2013, Kumar et al. reported the first FPSC based on polyethylene terephthalate (PET) substrate with PCE of 2.62% prepared by using low-temperature processed ZnO nanorods as electron transport layers (ETLs) [25]. After that, many efforts have been made to improve the performance of FPSCs by optimizing the critical issues specifically for flexible devices (Fig. 2). Among these efforts, some breakthroughs on the materials and structure designs play critical roles on the evolution of efficiency and mechanical flexibility of FPSCs. For example, the efficiency of PSCs on flexible substrates is highly suppressed due to the difficulty of preparing conventional

inorganic transport layers through low temperature process. Hence, Snaith et al. introduced poly(3,4-ethylenedioxythiophene): polystyrene sulfonate (PEDOT:PSS) as an organic hole transport layer (HTL) into an inverted device structure to release the dependence on inorganic transport layers and the PCE of FPSCs was improved to 6.4% [26]. Liu et al. improved the efficiency to 10.2% by using a thin film of ZnO nanoparticles as an ETL [27]. Kim et al. fabricated FPSCs with a best PCE of 12.2% based on a compact TiO_x layer (20 nm) prepared by plasma enhanced atomic layer deposition at 80 °C [28]. They also performed the bending durability test on the devices for the first time. Shin et al. employed Zn₂SnO₄ nanoparticles as an ETL to further improve the PCE to 15.3% and the temperature for whole process is below 100 °C [29]. Yoon et al. utilized graphene as a bottom electrode to prepare super-flexible solar cells [30]. Due to the high transmittance and conductivity of graphene electrode, the efficiency was increased to 16.8%. In addition to the quality of transport layers, the crystallinity of perovskite films is also important for the photovoltaic performance of FPSCs. Feng et al. prepared perovskite films with large grains and low defect density by using dimethyl sulfide (DS) as an additive [31]. The efficiency was enhanced to 18.40%. Wu et al. used NMP and MACl as synergistic additives to optimize FAPbI₃ perovskites on flexible substrates. The efficiency was enhanced to 19.36% [32]. Recently, the efficiency was improved to 21.10% by using artemisinin to passivate the defects in the perovskite films [33].

Besides efficiency, the mechanical flexibility of FPSCs is another important issue. Deformable and stretchable FPSCs can be realized by employing flexible substrates with high bending durability. Park et al. employed a shape recoverable polymer as flexible substrates to successfully fabricate highly deformable FPSCs [36]. The FPSCs could keep about 60% of their initial value after 50 cycles of complete



Fig. 1. a) A photo of solar powered outdoor flight, b) solar powered tents, c) smart integrated building. d) Photographs of wearable PSCs as a power source to power a smartwatch. e) A photograph of a solar powered wearable sensor.

Part (c) Reprinted with permission from [20]. Copyright 2018, Elsevier Ltd. Part (d) Reprinted with permission from [21] Copyright 2019, Royal Society of Chemistry. Part (e) Reprinted with permission from [24]. Copyright 2019, Elsevier Ltd.

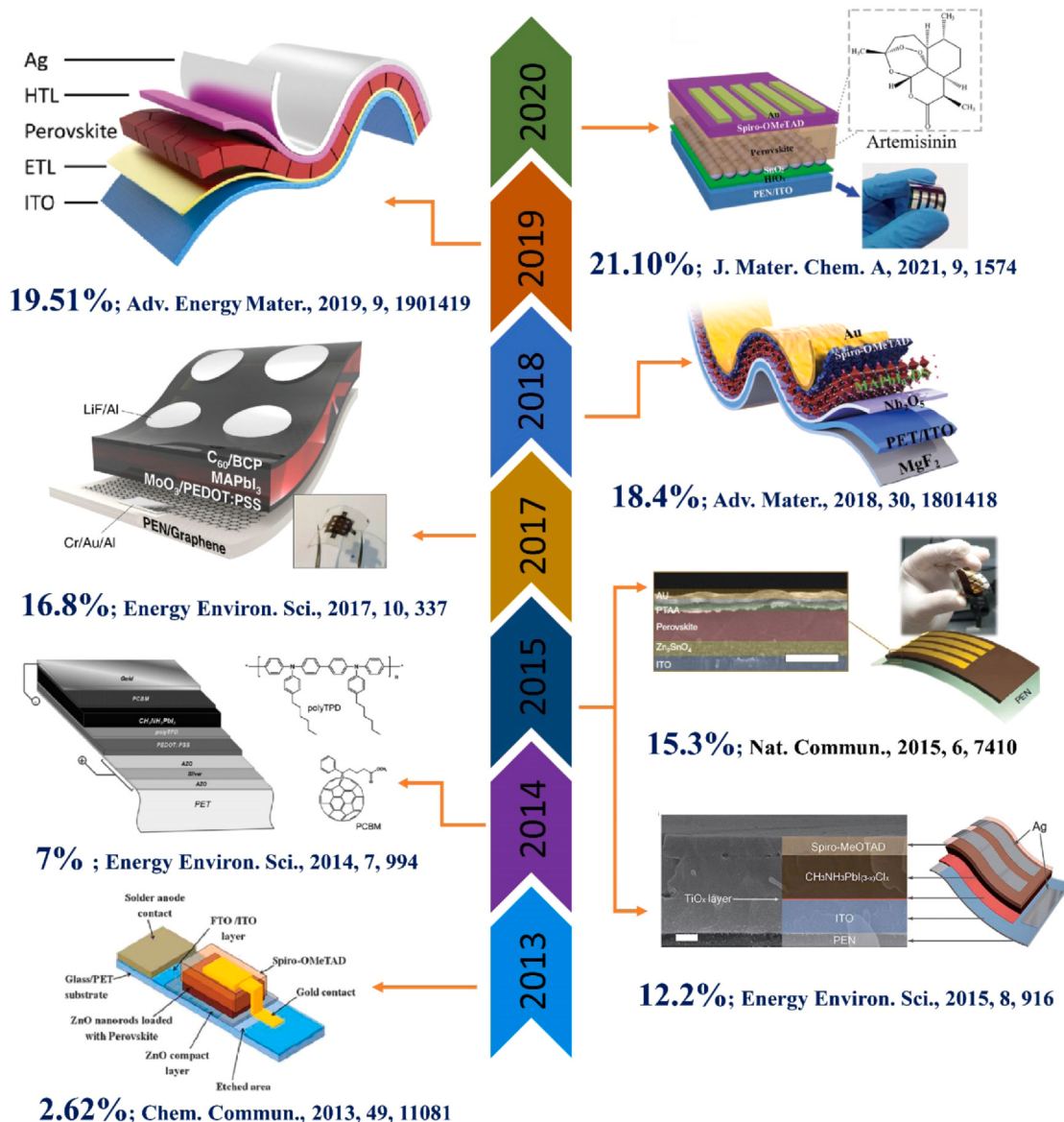


Fig. 2. The efficiency evolution of FPSCs from 2013 to 2020.

Reprinted with permission from [25,28–31,33–35]. Copyright 2013, 2014, 2015, 2016, 2021, Royal Society of Chemistry. Copyright 2018, 2019, John Wiley & Sons, Inc. Copyright 2015, Nature Publishing Group.

crumpling and shape recovery. Kaltenbrunner et al. realized a stretchable and lightweight FPSC with more than 12% PCE by using a thin PET substrate with the thickness of 1.4 μm [18]. The flexible devices could keep the initial performance after about 40% compression. Moreover, due to the thin thickness of complete device, the power per weight could reach 23 Wg⁻¹, which is the highest value in all photovoltaic technologies.

Low cost, high productivity, and large-scale fabrication are prerequisites for the commercialization of perovskite photovoltaic technology [37,38]. R2R coating is an efficient way to meet the requirements. Galagan et al. made efforts to prepare FPSCs by a slot die R2R coating method. The efficiency of fabricated devices could reach 14.5% with a mask area of 0.04 cm² [39]. Bu et al. slot-die printed SnO₂ film with high quality on flexible substrates. The prepared FPSC module with an area of 5 × 6 cm² demonstrated a PCE of 15.22% [40].

So far, the highest efficiency of FPSCs is above 21%, which however is much lower than the record value for rigid PSCs. The reasons for the relatively lower efficiency of FPSCs compared with rigid counterparts can be summarized as follows. 1) The high roughness

and easy deformation of polymer substrates would deteriorate the quality of adjacent charge transport layers (CTLs) and perovskite films, leading to low performance of FPSCs [35,41]. 2) The high sheet resistance and low optical transmittance of flexible substrates lead to low FF and J_{sc} of FPSCs, which is more obvious for large-scale fabrication [42]. 3) The low-temperature process (~100 °C) required by flexible substrates leads to lower crystallinity of CTLs and perovskite films, which results in lower efficiency of devices [43]. In the past two years, the highest efficiency of FPSCs has been boosted to 21.10% and several significant advances have been achieved [33]. Therefore, a comprehensive review is needed to systematically summarize the developments of FPSCs, especially in recent years, which has been rarely reported in other reviews with the similar topic [16,44,45]. Herein, this review mainly focuses on the strategies for enhancing device efficiency and mechanical flexibility based on new materials and fabrication technologies suitable for low temperature process. Since the plastic substrates are permeable to water and oxygen, which leads to the poor long-term stability of FPSCs, efforts in the encapsulation technologies to overcome this issue are

Table 1

The photovoltaic performance of FPSCs based on different flexible substrates.

| Substrate | Device structure | PCE (%) | Ref. |
|---------------------------|--------------------------------------------------------------------------------------------------------------------------|---------|------|
| Flexible glass | Willow galss/ITO/ZnO/Perovskite/Spiro-OMeTAD/Gold | 12.06 | [46] |
| Flexible glass | MgF ₂ / Willow glass/ITO/PTAA/MAPbI ₃ /C ₆₀ /BCP/Cu | 19.72 | [47] |
| PET | MgF ₂ /PET/ITO/Nb ₂ O ₅ /MAPbI ₃ -dimethyl sulfide/Spiro-OMeTAD/Au | 18.40 | [31] |
| PET | PET/ITO/TiO _x /MAPbI ₃ :C-PCBOD/Spiro-OMeTAD/Au | 18.10 | [48] |
| PET | PET/PEDOT:PSS/MAPbI ₃ /C ₆₀ /BCP/Cu/Parylene | 17.03 | [49] |
| PET | PET/ITO/PEDOT:EVA/Perovskite/PCBM/BCP/Ag | 19.87 | [17] |
| PET | PET/PEDOT:PSS/NiO _x /Perovskite:s-GO/PCBM/BCP/Ag | 20.56 | [50] |
| PET | PET/Ni-mesh:PEDOT:PSS PH1000:PEDOT:PSS-NiO _x /MAPbI ₃ :C-PCBOD/PCBM/BCP/Ag | 17.30 | [51] |
| PET | PET/ITO/SnO ₂ /Peovskite/Spiro-OMeTAD/Au | 19.10 | [52] |
| PET | PET/AuCl ₃ doped Graphene/APTES/PEDOT:PSS/MAPbI ₃ /PCBM/AI | 17.90 | [53] |
| PET | PET/Graphene/P3HT/MAPbI ₃ /PCBM/Ag | 11.50 | [54] |
| PET | PET/IZO/PTAA/Perovskite/PCBM/Cr/Carbon | 15.18 | [55] |
| PET | PET/Graphene/ethylene glycol (EG)/ZnO/PCBM/MAPbI ₃ /PTAA/Au | 12.61 | [56] |
| PEN | PEN/ITO/SnO ₂ /FAPbI ₃ with MACl/Spiro-OMeTAD/Au | 19.38 | [57] |
| PEN | PEN/ITO/SnO ₂ /FAPbI ₃ with MABr/Spiro-OMeTAD/Au | 18.50 | [58] |
| PEN | PEN/ITO/HfO _x /SnO ₂ /Perovskite:artemisinin/Spiro-OMeTAD/Au | 21.10 | [33] |
| PEN | PEN/Graphene/MoO ₃ /PEDOT:PSS/MAPbI ₃ /C ₆₀ /BCP/LiF/AI | 16.80 | [30] |
| PEN | PEN/ITO/SnO ₂ /Zn ₂ SnO ₄ /Perovskite/Spiro-OMeTAD | 20.70 | [43] |
| PEN | PEN/ITO/PTAA/PFN-Br/Perovskite/C60/BCP/Cu | 20.0 | [59] |
| PI | PI/ITO/ZnO/Perovskite/PTAA/Au | 15.50 | [60] |
| PI | PI/Ag NPs/PH1000:PEDOT:PSS 4083/MAPbI ₃ /PCBM/PEI/Ag | 10.41 | [61] |
| PI | PI/Cu grid/Graphene/PEDOT:PSS/Perovskite/PC61BM/ZnO/Ag | 16.40 | [62] |
| PDMS | PDMS/hc-PEDOT:PSS/AI4083/Perovskite/PCBM/PEI/hc-PEDOT:PSS/PDMS | 19.15 | [63] |
| Ti foil | Ti/compact TiO ₂ / mesoporous TiO ₂ /MAPbI ₃ /Spiro-OMeTAD /Ag | 6.15 | [64] |
| Ti foil | Ti/compact TiO ₂ / mesoporous TiO ₂ /MAPbI ₃ /Spiro-OMeTAD /Ag/ITO | 11.01 | [65] |
| Ti foil | Ti/TiO ₂ /Al ₂ O ₃ /MAPbI ₃ /Spiro/PEDOT:PSS/conductive adhesive/Ni mesh/PET | 10.30 | [66] |
| Ti foil | Ti/oxidized Ti/Perovskite/Spiro/Au | 14.7 | [67] |
| Ti foil | Ti/TiO ₂ /Perovskite/PTAA/Graphene/PDMS | 15.0 | [68] |
| Cu foil | Cu/Cu/Perovskite/ZnO/Ag | 12.80 | [69] |
| Cellophane paper | Cellophane/OMO/CTPA/MAPbI ₃ /Spiro-OMeTAD /Au | 13.19 | [70] |
| Nanocellulose paper (NCP) | NCP/PEDOT:PSS/PEDOT:PSS 4083/Perovskite/PCBM/AI | 4.25 | [71] |
| b-CNF | b-CNF/IZO/PEDOT:PSS/Perovskite/PCBM/Ag | 11.68 | [72] |

summarized. The progress in large-scale fabrication by R2R method are also reviewed, which is critical to commercialization in the future. In the end, conclusion is made and perspective on the future development of FPSCs is presented.

Flexible substrates

Flexible substrate is a key component of a flexible device since the following layer depositions are highly dependent on the chemical and mechanical properties of the substrate. To be an ideal flexible substrate for a photovoltaic device, it should have high optical transmittance, high thermal tolerance, robust mechanical durability, high resistance to chemical solvents, good oxygen and water barrier properties, and low surface roughness. Several different substrates have been explored to meet such requirements, leading to FPSCs with high efficiency and good mechanical flexibility. However, no substrate could simultaneously satisfy all the requirements. The photovoltaic performance of FPSCs base on different substrates are summarized in Table 1.

Flexible glass

There are mainly three types of flexible substrates employed in the fabrication of FPSCs, including flexible glasses, metal foils, and polymer substrates. A glass substrate with a thickness lower than several hundred micrometers could become mechanically flexible. This type of substrate could meet most of the requirements, such as high transmittance, strong thermal tolerance (>600 °C), impermeability to water and oxygen, and compatibility with almost all chemical solvents. Tavakoli et al. first used willow glass with a thickness of 50 µm as flexible substrates to prepare FPSCs and achieved efficiency up to 12.06% [46]. The PCEs of the flexible devices have little degradation (~0.5%) after 200 bending cycles with a radius of 4 cm. The smooth and indeformable surfaces of the flexible glass

substrates under high temperature enable large-area fabrication of the devices. Flexible perovskite photovoltaic modules (42.9 cm²) with a record PCE of 15.86% were realized by blade-coating high quality perovskite films with NH₄Cl additive on the flexible glass substrates [47]. The FPSCs with 8 mm² could demonstrate a best PCE of 19.72% (Fig. 3). However, the fragility and relatively high cost of ultrathin glass substrates limit their wide use as flexible substrates in practical applications.

Metal foils

Metal foils are supposed to be promising flexible substrates due to their high flexibility, thermal resistance and conductivity. They can simultaneously work as flexible substrates, bottom electrodes, and even transport layers, which significantly simplify the fabrication process. However, the opaque nature of metal foils requires that the top electrodes of the devices must be transparent, which is a major obstacle in device fabrication. Thus, much efforts have been devoted to exploring top electrodes with high transparency and conductivity for FPSCs on metal foils.

Lee et al. introduced Ti foils as flexible substrates to prepare ITO-free FPSCs for the first time with a device structure of Ti/compact TiO₂/mesoporous TiO₂/perovskite/spiro-MeOTAD/Ag [64]. Due to the high temperature resistance of Ti foil, the TiO₂ layers could be well crystallized at high temperature in a furnace. An ultrathin Ag film with an optimum thickness of only 12 nm served as a top semi-transparent electrode where sunlight enters. They noticed that a thinner Ag film has poor conductivity, which leads to lower FF and J_{sc}, while a thicker film would decrease its transmittance and result in a lower short-circuit current. The transmittance of the optimum Ag film is about 45% lower than that of an FTO electrode at a wavelength range of 450–750 nm, leading to a best efficiency of 6.15%. The flexible devices show good mechanical durability by retaining about 98.5% of the initial PCE after 100 bending cycles at a bending

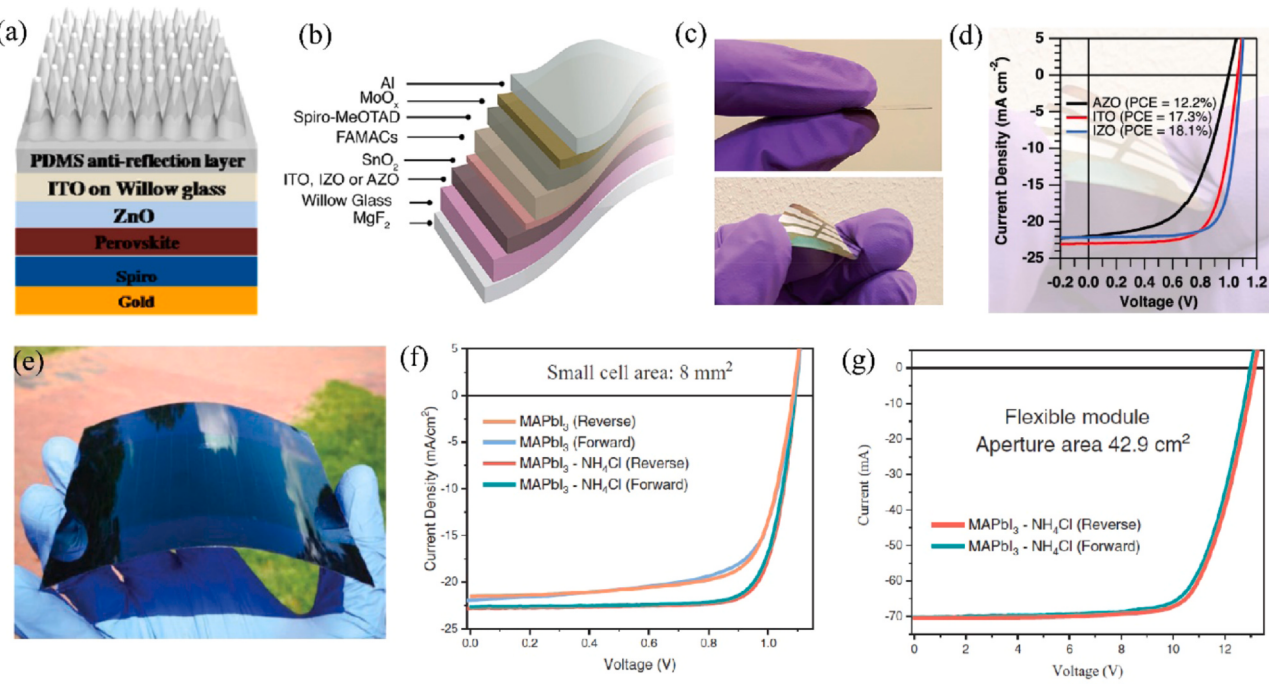


Fig. 3. a) Schematic structure of a FPSC based on a flexible glass substrate with a PDMS anti-reflection layer. b) Schematic representation of a device architecture for FPSCs based on flexible glass substrates. c) A photo of a FPSC based on a flexible glass substrate. d) J-V curves of FPSCs with three different bottom electrodes. e) J-V curve of small-area blade-coated FPSCs with a champion PCE of 19.72%. f) J-V curve of a blade-coated flexible perovskite modules with a champion PCE of 15.86%.

Part (a) Reprinted with permission from [46]. Copyright 2015, American Chemical Society. Part (d) Reprinted with permission from [73]. Copyright 2017, American Chemical Society. Part (f) Reprinted with permission from [47]. Copyright 2019, John Wiley & Sons, Inc.

radius of 6 mm. Thus, the transmittance and conductivity of top electrodes are very important for the photovoltaic performance of FPSCs on metal foils. They further used more transparent ITO as a top electrode by sputtering to enhance the light absorption of the perovskite layer [65]. Furthermore, an ultrathin Ag layer with a thickness of 1 nm was embedded between spiro-MeOTAD and ITO to decrease the sheet resistance of ITO electrode from 35.48 to 7 Ω/□. The discontinuous ultra-thin Ag film enabled higher diffusive transmittance. Based on these techniques, the PCE of FPSCs with Ti substrates was increased to 11.01%. Moreover, a transparent top electrode with a more complicated structure (PEDOT:PSS/conductive adhesive/Ni mesh) was used to prepare FPSCs on Ti substrates and efficiency of 10.3% was achieved [66].

Thermally oxidized the surfaces of Ti substrates to form TiO₂ ETLs could simplify the device fabrication process and save materials cost. Han et al. reported that a decrease in the concentration of oxygen vacancies in the TiO₂ could enhance the electron collection efficiency [67]. The FPSCs with top transparent electrode of Au (7 nm)/ Cu (1 nm) demonstrated the champion PCE of 14.9%. Due to the high crystalline quality of TiO₂ layer, FPSCs could maintain 100% of their initial PCEs after 1000 bending cycles at a bending radius of 4 mm. Heo et al. used TiO₂ as transport layer formed by anodizing Ti substrates and tri-layer graphene layers as top electrodes to prepare FPSCs and efficiency of 15.0% was obtained measured with a mask area of 1 cm² (Fig. 4a–c) [68].

Nejand et al. selected copper foils as flexible and conductive substrates due to the same work function as ITO (Fig. 4d) [69]. Moreover, Cul as a HTL could be formed by iodinating copper substrates. The FPSCs with an inverted structure of Cu/Cul/perovskite/ZnO/Ag nanowires exhibited 12.80%. Although metal foils have several advantages as flexible substrates, the absence of more

suitable top transparent electrodes with better conductivity and flexibility hinders the development of FPSCs prepared on metal foils.

Polymer substrates

Polymer substrates, such as PET, polyethylene naphthalate (PEN), and polyimide (PI), are mostly used flexible substrates due to the high bendability, light weight, low cost, high corrosion resistance, high optical transparency, and R2R processability. However, the thermal resistances of these polymer substrates are relatively poor. The property parameters for different polymeric substrates are shown in Table 2 [74]. The glass transition temperatures of PET, PEN, and PI are 78, 120 and 200 °C, respectively. Deformation of substrates would occur when the processing temperature is changed too much. The resistance of ITO deposited on a PET substrate has a significant increase when the annealing temperature is over 200 °C. Therefore, the whole process of devices fabrication must be conducted at a low temperature. Considering the required processing temperatures of perovskite films are normally lower than 150 °C, more efforts have been devoted to preparing charge transport layers with high quality at low temperatures to improve the photovoltaic performances of FPSCs. Another drawback of polymer substrate is the poor water and oxygen barrier property. They have higher water and oxygen transmission rate than that of glass and metal foil substrates [75]. Therefore, further encapsulation is highly desirable to achieve long-term stability. So far, polymer substrates (PET and PEN) are still the most prevalent choices for FPSCs due to the resultant high efficiency and the ease of fabrication. Thus, the following parts are mainly focusing on FPSCs prepared on polymer substrates. In addition, some biodegradable materials have also been used as flexible substrates for FPSCs, such as, cellophane paper and bamboo (Fig. 4e and f) [71,72].

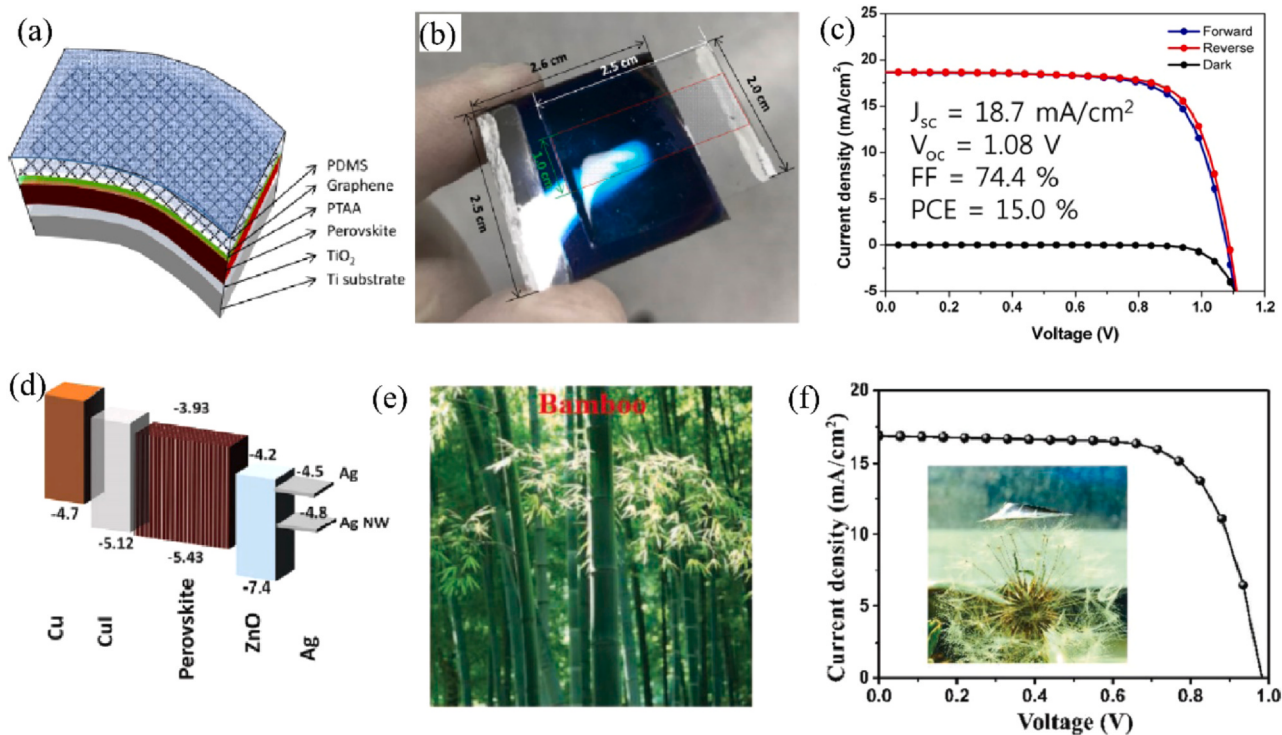


Fig. 4. a) Schematic device structure of a FPSC based on Ti foil substrate. b) photograph of a real flexible device based on a Ti substrate. c) J-V curve of a FPSC based on Ti substrate. d) Energy level diagram of Cu/CuI/CH₃NH₃PbI₃/ZnO/Ag. e) photograph of bamboo. f) J-V curves of a FPSC based on a bamboo substrate with a champion PCE of 11.68%. Part (c) Reprinted with permission from [68]. Copyright 2018, American Chemical Society. Part (d) Reprinted with permission from [69]. Copyright 2016, Royal Society of Chemistry. Part (f) Reprinted with permission from [72]. Copyright 2019, John Wiley & Sons, Inc.

Table 2
Comparison between flexible polymeric substrates.

| Substrate | PI | PET | PEN | PDMS |
|------------------------------|------------------------|-------------------------|---------------------------|------------------------|
| T _g (°C) | 155–270 | 70–110 | 120–155 | –125 |
| T _m (°C) | 250–452 | 115–258 | 269 | – |
| Density (g/cm ³) | 1.36–1.43 | 1.39 | 1.36 | 1.03 |
| Vol.Res. (Ω.cm) | 1.5 × 10 ¹⁷ | 1.0 × 10 ¹⁹ | 10 ⁵ | 1.2 × 10 ¹⁴ |
| Modulus (MPa) | 2.5 × 10 ³ | 2–4.1 × 10 ³ | 0.1–0.5 × 10 ³ | 1 |
| WorkTemp. (°C) | Up to 400 | –50–150 | – | –45–200 |
| CET (ppm/°C) | 8–20 | 15–33 | 20 | 310 |
| Water absorption (%) | 1.3–3.0 | 0.4–0.6 | 0.3–0.4 | >0.1 |
| Solvent resistance | Good | Good | Good | Poor |
| Dimensional stability | Fair | Good | Good | Good |

T_g-glass transition temperature, T_m-melting temperature, CET-coefficient of thermal expansion [74].

Influence of flexible substrates on mechanical strain in devices

In a FPSC, the stain on the surface of a bent device is given by [70,76]:

$$\epsilon = \frac{t}{2R} \quad (1)$$

where t is the thickness of the device and R the curvature radius. The device thickness of a FPSC is mainly contributed by its flexible substrate. Thus, a flexible substrate with a smaller thickness can lead to a lower strain in the active layer of the PSC prepared on its surface. In addition, the mechanical property of the substrate is critical to the mechanical stain in the device. The distribution of strain (ϵ) along z axis (surface normal) in a bent device with a structure of k layers and a radius of curvature R is given by the following equation [77]:

$$\epsilon(z, R) = \frac{z - z_{NA}}{R} \quad (2)$$

where z_{NA} is the position of the neutral axis of the structure with no strain, which is given by:

$$z_{NA} = \frac{\sum_{k=1}^n E_k^* t_k z_k}{\sum_{k=1}^n E_k^* t_k} \quad (3)$$

$$E_k^* = \frac{E_k}{1 - v_k^2} \quad (4)$$

where each layer k has a thickness t_k , a Young's modulus E_k and a Poisson's ratio v_k .

Based on the above relationships, the strain distribution in a device is related to the position of the neutral axis plane of the structure. A substrate with lower thickness and Young's modulus could decrease the strain in a bent device by tuning the position of the neutral axis plane [76,78]. For FPSCs, exploring a flexible substrate with suitable thickness and Young's modulus to make the neutral axis plane locate on the perovskite layer could substantially enhance the mechanical flexibility of devices.

According to the above theory, Lee et al. systematically investigated the relation between crack formation and the strain applied to perovskite films by adjusting the thickness of PET substrates (2.5, 30, and 100 μm) [49]. It was found that no cracks appeared at a perovskite film deposited on a 2.5 μm-PET after 1000 cycles bending at a radius of 0.5 mm. In comparison, many cracks formed at perovskite films deposited on 30 μm and 100 μm-PET. Moreover, the perovskite films on 100 μm-PET had more cracks than that on 30 μm thick PET. This phenomenon is due to the lower strain in perovskite films induced by thinner substrates. The FPSCs based on PET substrates with a thickness of 2.5 μm demonstrated a champion PCE of 17.3%. These ultra-flexible devices could maintain their initial performance after 10,000 bending cycles at a bending radius of 0.5 mm. A parylene layer with a thickness of 2.3 μm was coated on top of devices to further improve the mechanical flexibility by tuning the position of neutral plane to locate on perovskite layers. As a result,

Table 3

The photovoltaic performance of FPSCs based on different bottom transparent electrodes.

| Electrode | Device structure | PCE (%) | Ref. |
|------------|-----------------------------------------------------------------------------|---------|-------|
| Ag NWs | Ag nanowires/GO/PEDOT:PSS/Perovskite/PCBM/PFN-P1/Ag | 7.92 | [88] |
| Ag NWs | AgNWs/PEDOT:PSS/Perovskite/PCBM/Al | 11.0 | [92] |
| Ag NWs | AgNWs/PEDT:PSS1000/PEDOT:PSS4083/Perovskite/PCBM/Ag | 15.18 | [93] |
| Ag NWs | a-AZO/AgNW/AZO/ZnO/Perovskite/Spiro/Au | 11.23 | [90] |
| Ag NWs | AgNW/ITO/PEDOT:PSS/Perovskite/PCBM/BCP/Ag | 14.15 | [89] |
| Cu NWs | CuNW/ITO/PEDOT:PSS/Perovskite/PCBM/BCP/Ag | 12.95 | [89] |
| Cu NWs | AZO/CuNW/g-AZO/SnO ₂ /Perovskite/Spiro/Au | 14.18 | [91] |
| Ag mesh | Ag-mesh/PH1000/PEDOT:PSS4083/Perovskite/PCBM/Al | 14.0 | [94] |
| Cu grid | Cu grid/Graphene/PEDOT:PSS/Perovskite/PCBM/ZnO/Ag | 16.4 | [62] |
| Cu grid | Cu grid/PH1000/Cu:NiO _x /Perovskite/PCBM/Cu | 13.58 | [95] |
| SWNT | SWNT/MoO ₃ /PEDOT:PSS/Perovskite/C ₆₀ /BCP/LiF/Al | 12.8 | [102] |
| SWNT | HNO ₃ -SWNT/PEDOT:PSS/Perovskite/PCBM/Al | 6.32 | [101] |
| Graphene | Graphene/MoO ₃ /PEDOT:PSS/Perovskite/C ₆₀ /BCP/LiF/Al | 14.2 | [102] |
| Graphene | Graphene/TiO ₂ /PCBM/Perovskite/Spiro/Carbon nanotubes | 11.9 | [103] |
| Graphene | Graphene/MoO ₃ /PEDOT:PSS/Perovskite/C ₆₀ /BCP/LiF/Al | 16.8 | [30] |
| Graphene | Graphene/P3HT/Perovskite/PCBM/Ag | 11.5 | [100] |
| Graphene | Graphene-AgNWs/SnO ₂ /MAPbI ₃ /Carbon | 9.73 | [109] |
| Graphene | Graphene/MoS ₂ /MAPbI ₃ /PTAA/Au | 12.92 | [110] |
| AZO/Ag/AZO | AZO/Ag/AZO/PEDOT:PSS/PolyTPD/Perovskite/PCBM/Au | 7.0 | [34] |
| PEDOT:PSS | PEDOT:PSS-Zn(TFSI) ₂ /Al4083/Perovskite/PCBM/Ag | 19.0 | [107] |
| PEDOT:PSS | PEDOT:PSS/Perovskite/PCBM/Cr/Cr ₂ O ₃ /Au | 12.0 | [18] |
| PEDOT:PSS | PEDOT:PSS-lycol/Al4083/Perovskite/PCBM/PEI/PEDOT:PSS | 15.61 | [21] |

the FPSCs with a parylene layer could retain 88% of initial performance after more than 100 cycles of complete crumpling or folding.

Low temperature processable transparent conductive electrodes

In the development of FPSCs, the exploration of transparent conductive electrodes with high conductivity is always the main theme. An ideal bottom electrode should be highly transparent, mechanically flexible, highly conductive, low temperature processable, and chemically stable. The photovoltaic performance of FPSCs based on different bottom electrodes are summarized in Table 3.

Transparent conductive oxide

Indium tin oxide (ITO) is the most frequently used material for transparent electrodes. High-quality ITO film can be deposited on PET and PEN substrates by pulsed laser deposition (PLD) or magnetron sputtering methods [79]. The sheet resistances of ITO/PET or ITO/PEN could reach about $15\ \Omega/\square$, which is close to $10\ \Omega/\square$ for ITO/glass. Zardetto et al. had systematically investigated the optical transmittance and the thermal and mechanical stability of ITO/PET and ITO/PEN [42]. The transmittance of ITO/PET and ITO/PEN is a little bit lower than that of glass counterparts in the visible light range. In the ultraviolet light range, the transmittance is much lower due to the strong absorption of polymer substrates. For thermal stability, ITO/PEN has unchanged resistance ($15\ \Omega/\square$) when it is annealed up to 235 °C. At 250 °C, the resistance increases for almost 20-fold due to the deformed PEN substrate. For ITO/PET, the critical temperature is only 150 °C (Fig. 5a). Both ITO/PET and ITO/PEN show degradation when they are bent at curvature radius lower than a critical value (Fig. 5b and c). Tensile stress could lead to more serious degradation in comparison with compressive stress due to the generation of cracks in ITO films. Highly conductive PEDOT:PSS has been employed to be deposited on ITO films to increase the bending stability by filling the cracks as an electric bridge.

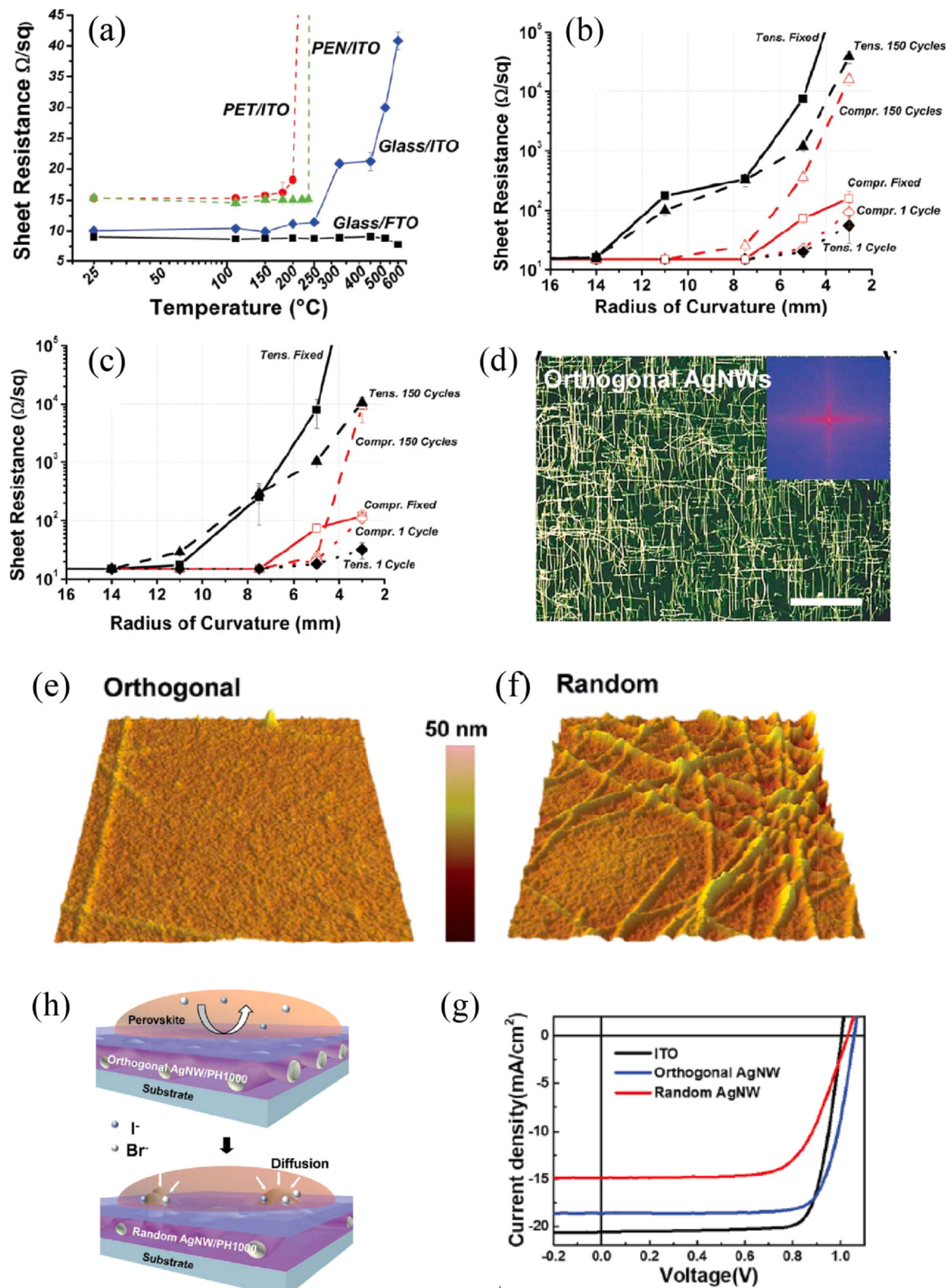
Other transparent conductive oxide (TCO) electrodes have also been explored. Dou et al. deposited different kinds of TCO layers on flexible glass substrates to investigate the effect of TCO substrates on the efficiency of FPSCs [73]. The PCE of the devices with indium zinc oxide (IZO) transparent electrodes reached 18.1%; FPSCs based on ITO demonstrated PCE of 17.3%, while devices based on aluminum-doped zinc oxide (AZO) showed PCE of only 12.2%. The relatively

lower PCE based on AZO is due to the dramatical change of the stoichiometry of perovskite films grown on AZO.

Although the FPSCs with highest efficiency so far are prepared with ITO electrodes on PET substrates, the intrinsically brittle property of ITO is a major obstacle for the flexible applications [80]. Moreover, the high cost of ITO material is another issue hindering the commercialization of PSCs. A kind of electrodes with a double-sandwich structure were explored to replace ITO electrodes in FPSCs. Carmona et al. used a stack of thin layers including Al doped ZnO (AZO), silver and AZO as a transparent electrode in the fabrication of FPSCs [34]. This electrode has transmittance of 81% in the visible range and a low sheet resistance of $7.5\ \Omega$. The devices could achieve a best PCE of 7% and retained 98.5% of initial PCE after 50 bending cycles at a bending radius of 2.75 cm.

Metal nanowires

Solution-processable metal nanowires are promising candidate materials for transparent and conductive electrodes due to the high conductivity, flexibility and transparency [81]. Silver nanowires (NWs) are widely used as transparent electrodes due to the superior electrical properties of Ag materials and upscaling synthesis. Generally, the conductivity of Ag NWs could be improved when the length and diameter of each individual wire increases. Ag NWs can be synthesized by hard-template and soft-template methods [82]. The conductivity and transmittance could even be better than those of ITO electrodes [83–86]. However, the random deployment of nanowires could lead to a highly rough surface, which results in serious leakage in PSCs. Moreover, the halides in perovskites would chemically react with Ag and lead to serious degradation of device performance [81,87]. Thus, many strategies have been introduced to overcome the drawbacks. Lu et al. used graphene oxide (GO) flakes deposited on Ag NWs films as an anti-corrosive barrier, which can effectively block the penetration of halides into the electrodes [88]. Furthermore, due to the suitable work function alignment and more wetting property of the surfaces of Ag NWs electrodes, resultant FPSCs demonstrated a champion PCE of 7.92%. Im et al. deposited crystalline ITO on the Ag NWs and Cu NWs electrodes to improve the conductivity and chemical stability [89]. The FPSCs showed efficiencies of 14.15% and 12.95% for ITO/Ag NWs and ITO/Cu NWs, respectively. An electrode with a sandwich structure of conductive oxide/Ag NWs/conductive oxide enables high transmittance and conductivity. A pinhole-free amorphous aluminum doped zinc oxide



caption on next page

Fig. 5. a) Room temperature sheet resistance of conductive PET/ITO, PEN/ITO foils and glass/ITO, glass/FTO substrates after undergoing a thermal treatment at different temperatures for 30 min. Sheet resistance of b) PET/ITO and c) PEN/ITO as a function of radius of curvature under tensile (in black) and compressive (in red) strain for three different situations: measured on a curved cylindrical surface (squares-line); after 150 (triangles-dashed) and 1 (diamonds-dotted) bending cycles measured flat. d) Dark-field optical microscopy image of the orthogonal AgNW arrays; the corresponding FFT pattern is shown in the inset. AFM images of the surface of PEDOT:PSS (Al4083) coated onto e) a PH1000/orthogonal AgNW electrode and f) a PH1000/random AgNW electrode, respectively. g) Schematic of silver halide formation in PSCs fabricated on random and orthogonal AgNW electrodes. h) J-V characteristic of FPSCs with ITO, orthogonal AgNW, and random AgNW electrodes. The PCEs are 16.25%, 15.18%, and 10.43%.

Part (c) Reprinted with permission from [42]. Copyright 2011, John Wiley & Sons, Inc. Part (h) Reprinted with permission from [93]. Copyright 2019, Royal Society of Chemistry.

(a-AZO) was employed as a protection layer deposited on AgNWs network to fabricate a-AZO/AgNW/AZO composite electrodes [90]. The electrodes demonstrated a transmittance of 88.6% at 550 nm and a sheet resistance of $11.86 \Omega \text{sq}^{-1}$. The best PCE of resultant FPSCs reached 11.23%. Yang et al. used Al-doped ZnO (AZO)/Cu NWs/AZO composite electrode to fabricate FPSCs and obtained a PCE of 14.18%, which is higher than the efficiency (12.34%) of the device without an AZO layer [91]. Moreover, the sandwich structures can also improve the bendability of Ag NWs-based electrodes.

Sears et al. prepared FPSCs with an efficiency of 11% based on PEDOT:PSS coated Ag NWs by R2R slot die method [92]. Considering that the random deployment of metal NWs could lead to rough surfaces of the electrodes, Kang et al. prepared Ag NWs electrodes with orthogonal deployment of the NWs [93]. The smooth morphologies of the obtained electrodes boosted the PCE of the devices to 15.18%, which is much higher than the efficiency (10.43%) for FPSCs based on random Ag NWs electrodes (Fig. 5d–h).

Metal grids

Metal grid electrodes have been investigated as bottom window electrodes for FPSCs. Due to the rough surface and chemical instability with perovskites, a cap layer is usually required. Li et al. successfully fabricated FPSCs based on PET substrates with

embedded hexagonal Ag-mesh electrodes [94]. Highly conductive PEDOT:PSS (PH1000) was coated on the Ag-mesh electrodes to improve the conductivity and flexibility (Fig. 6a–c). The hybrid PET/Ag-mesh/PH1000 electrode exhibited a sheet resistance of $3 \Omega/\square$ and a transmittance of 82–86% in the visible region, and the PCE of resultant FPSCs reaches 14.0% (Fig. 6d). The devices demonstrate good stability under mechanical deformation, keeping over 95% of their initial efficiency after 5000 bending cycles at a curvature radius of 5 mm. Highly conductive PEDOT:PSS was also employed as a capping layer for Cu grid electrode and efficiency of 13.58% was achieved [95]. In addition, graphene was used as a capping layer to prepare a highly flexible electrode with a structure of PI/Cu grid/graphene [62]. The graphene layer could prevent metal and halide inter-diffusion in the devices and enhance the device long-term stability. The flexible devices could achieve a high efficiency of 16.4%. After 10,000 bending cycles at a radius of 5 mm, the device could maintain 94% of its initial PCE.

Carbon-based materials

Carbon-based materials, such as graphene and carbon nanotubes, have been explored as window electrodes due to their high conductivity and transmittance [96–98]. A single layer graphene film has a high transmittance of about 97.7% in the visible region, which

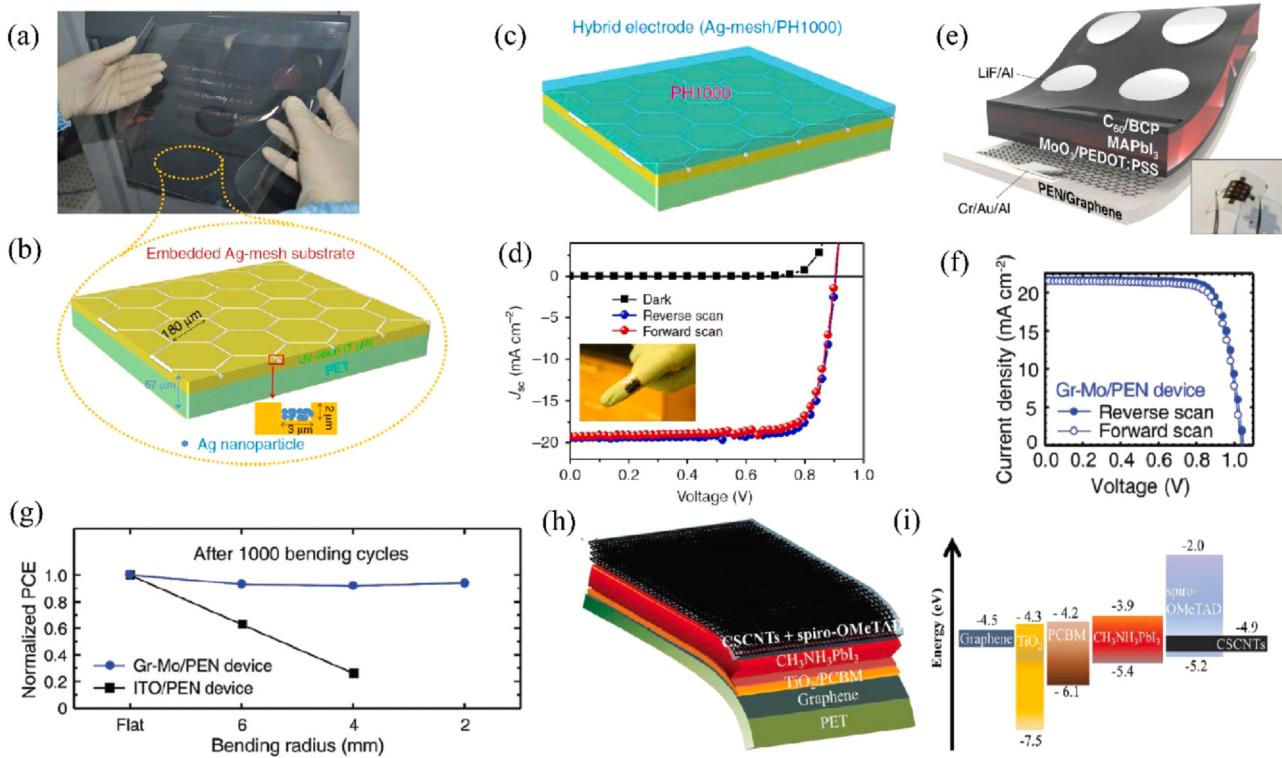


Fig. 6. a) An image of the large-area flexible PET substrate with embedded Ag-mesh. b) The structure of a flexible substrate with detail parameters. c) The diagram for the hybrid electrode (PET/Ag-mesh/PH1000). d) J-V curves for the champion flexible PET/Ag-mesh/PH1000/PEDOT:PSS/MAPbI₃/PCBM/Al solar cell with a PCE of 14%; Inset shows photograph of corresponding ultra-thin FPSC [94]. e) Device structure of graphene-based FPSCs (inset image: Photograph of a complete device). f) J-V curve of a FPSC with structure of PEN/Graphene/MoO₃/PEDOT:PSS/MAPbI₃/C₆₀/BCP/LiF/Al and a PCE of 16.8%. g) Normalized PCEs of Graphene and ITO-based devices measured after 1000 bending cycles with various bending radii: flat, 6, 4, and 2 mm. h) Device architecture of the all-carbon-electrode-based FPSCs. i) Energy levels of various device layers in FPSCs.

Part (g) Reprinted with permission from [30]. Copyright 2017, Royal Society of Chemistry. Part (i) Reprinted with permission from [103]. Copyright 2018, John Wiley & Sons, Inc.

is much higher than that of an ITO electrode [99]. Graphene was used by our group as transparent electrodes to fabricate FPSCs for the first time [100]. Large-area graphene was prepared by the conventional CVD method and transferred to flexible PET substrates. Double layer graphene and P3HT were employed as an electrode and an HTL in preparing FPSC and a PCE of 11.5% was achieved. Yoon et al. deposited MoO₃ with a thickness of 2 nm on graphene to introduce p-type doping and increase the conductivity of the graphene layer (Fig. 6e) [30]. The FPSCs based on MoO₃-graphene electrodes exhibited the best efficiency of 16.80% (Fig. 6f). The devices could retain about 85% of their initial efficiencies after 5000 bending cycles at a radius of 2 mm.

Jeon et al. first explored single-walled carbon nanotubes as transparent electrodes of FPSCs and obtained an efficiency of 6.32% [101]. The authors also compared the efficiency and flexibility of FPSCs based on graphene and single-walled carbon nanotubes (SWNTs) electrodes [102]. Due to the better morphology and transparency of graphene, the best efficiency of graphene-introduced FPSCs was 14.2%, which was higher than that of SWNTs counterparts (12.8%). However, SWNTs based FPSCs demonstrated better mechanical flexibility due to the randomly oriented entanglement of SWNTs. Luo et al. fabricated all-carbon-electrode based FPSCs with graphene as bottom electrodes and carbon nanotubes as top electrodes (Fig. 6h). The best efficiency can reach 11.9% [103]. The devices could retain over 90% of initial PCEs after 1000 h of continuous light soaking or 60 °C thermal stress in air.

PEDOT:PSS

PEDOT:PSS, a conductive polymer, has been investigated as a promising alternative for ITO electrodes due to the solution processability of the material at low temperature [104]. As-cast PEDOT:PSS films could have high conductivity up to 4000 S cm⁻¹ by various doping strategies [105]. Kaltenbrunner et al. used Dimethyl sulfoxide (DMSO) -doped PEDOT:PSS as bottom electrodes to prepare FPSCs on PET substrates with a thickness of 1.4 μm [18]. The ultrathin FPSCs demonstrated the best efficiency of 12.5% and record power-per-weight of 23 Wg⁻¹. Zhang et al. used nitric acid treated PEDOT:PSS films as both bottom and top electrodes by transferring method to prepare semitransparent FPSCs with the best efficiency of 10.3% [106]. Hu et al. used PEDOT:PSS with 5 wt% glycol and 0.5 wt% Zonyl FS-300 as electrodes and successfully fabricated FPSCs with a PCE of 15.01% and an area of 1 cm² [21]. The authors further enhanced the conductivity of PEDOT:PSS to over 4000 S/cm by using a novel fluorosurfactant dopant. The efficiency of FPSCs is boosted to 19.0% with a working area of 0.1 cm² [107]. Although PEDOT:PSS has been successfully applied as a transparent electrode material to prepare high-efficiency FPSCs, its acidic characteristic is an obstacle for achieving long-term stability of the FPSCs based on it [108].

Charge transport layers

In a PSC, high-quality charge transport layers could efficiently extract electrons and holes from interfaces and transport them to the corresponding electrodes, which is highly related to the band structure, morphology and carrier mobility of the charge transport layers [111]. The morphology of charge transport layers also significantly affects the growth and crystallization of perovskite films [112]. As mentioned in the introduction part, for FPSCs with a n-i-p structure, it is challenging to fabricate an ETL, such as TiO₂, SnO₂, or ZnO, at low temperature with high quality on flexible substrates. Generally, inorganic ETLs usually need high-temperature sintering to be fully crystallized to decrease the defects and improve the carrier mobility. However, high temperature annealing would destroy the flexible substrates. Therefore, various strategies have been developed to improve the extraction rates and transport capability of ETLs

processed at low temperature to enhance the photovoltaic performance of FPSCs. In comparison, it is more convenient to prepare organic HTLs like PEDOT:PSS and PTAA at low temperature for FPSCs. Inorganic HTLs such as NiO_x can lead to better device stability while low temperature processing is more difficult. The photovoltaic performance of FPSCs based on different ETLs and HTLs processed at low temperatures are summarized in Tables 4 and 5, respectively.

ZnO

ZnO was first employed as ETLs for FPSCs due to the high electron mobility, broad optical bandgap, suitable energy band alignment, and low temperature solution processability. Kumar et al. used electrodeposited ZnO compact layer and chemical bath deposited ZnO nanorods as ETLs to prepare FPSCs [25]. The whole processing temperature was lower than 100 °C while the best efficiency was only 2.62%. Low temperature processed ZnO compact layers demonstrate low mobility and high defect density, which are the main barriers for high-efficiency solar cells. Highly crystallized nanoparticles are promising alternatives that can overcome this problem. Liu et al. reported the use of ZnO nanoparticles with 5 nm in diameter as an ETL for FPSCs [27]. The ZnO nanoparticle layer could be deposited simply by spin coating without thermal annealing or sintering. Due to the high crystallinity of ZnO nanoparticle layer, the best efficiency of the flexible devices was boosted to 10.2%. Shin et al. used highly dispersed Zn₂SnO₄ nanoparticles as ETLs in FPSCs (Fig. 7a) [113]. The deposition of Zn₂SnO₄ layer significantly improved the transmittance of PEN/ITO substrate from 75% to 90% over the visible light range due to an anti-reflection effect and consequently the best efficiency was increased to 15.3% (Fig. 7b). They further boosted the efficiency to 16% by introducing Zn₂SnO₄ quantum dots onto the top of Zn₂SnO₄ nanoparticle layers [114]. Due to the low work function of Zn₂SnO₄ quantum dots, the build-in potential (V_{bi}) at the Zn₂SnO₄ quantum dots/perovskite interface was enlarged, which would lead to the improvement of the open-circuit voltage.

Although ZnO has superior electronic properties, the decomposition reaction at the ZnO/perovskite interface is a serious issue preventing the wide use [115,116]. The decomposition reaction is due to the presence of hydroxyl groups or residual organic acetate ligands on ZnO surface and proton-transfer reactions between ZnO and perovskite. Therefore, Jin et al. deposited an atomic-layer TiO₂ passivation layer on the ZnO layer to eliminate the perovskite decomposition [117]. The FPSCs based on this technique demonstrated an improved efficiency of 17.11%.

TiO₂

Low temperature processing of the mostly used TiO₂ ETLs have been investigated for applications in FPSCs. In comparison with ZnO, TiO₂ is a more stable material. Kim et al. formed an amorphous TiO_x compact layer with a thickness of 20 nm on a PEN substrate at 80 °C by plasma enhanced atomic layer deposition. The TiO_x layer showed fast electron transport and the resultant FPSCs exhibited a best PCE of 12.2% (Fig. 7c) [28]. In addition, a dense TiO₂ layer can be fabricated via magnetron sputtering method at room temperature. The prepared FPSCs showed a best efficiency of 15.07% [118]. Qiu et al. explored the fabrication of a TiO₂ layer by an electron beam evaporation, during which the temperature of the substrate and the thickness of the TiO₂ layer could be easily controlled [119]. The thickness of TiO₂ layer was optimized to obtain pinhole-free layers, which also led to the full coverage of perovskite layers above them. The efficiency of 13.5% was achieved in corresponding FPSCs. Giacomo et al. adopted a plasma-enhanced atomic layer deposition (PEALD) method to deposit TiO₂ as a compact layer and UV irradiated mesoporous TiO₂ layer as a scaffold to prepared FPSCs with a

Table 4

The photovoltaic performance of FPSCs based on different ETLs processed at low temperature.

| ETL | Device structure | PCE (%) | Ref. |
|-----------------------------------------------------------------|----------------------------------------------------------------------------------------------------|---------|-------|
| ZnO nanorods | ITO/ZnO compact/ZnO nanorods/Perovskite/Spiro-OMeTAD/Au | 2.62 | [25] |
| ZnO NPs | ITO/ZnO NPs/Perovskite/Spiro-OMeTAD/Au | 10.2 | [27] |
| ZnO | ITO/ZnO/Perovskite/PTAA/Au | 15.6 | [144] |
| ZnO | ITO/ZnO/TiO ₂ /Perovskite/Spiro-OMeTAD/MoO ₃ /Ag | 17.11 | [117] |
| Zn ₂ SnO ₄ (ZSO) | ITO/ZSO/Perovskite/PTAA/Au | 14.85 | [113] |
| ZSO NPs/ZSO QDs | ITO/ZSO NPs/ZSO QDs/Perovskite/PTAA/Au | 16.0 | [114] |
| ZSO NPs | ITO/ZSO NPs/PCBM/Perovskite/Spiro-OMeTAD/Ag | 11.61 | [145] |
| Li-SnO ₂ | ITO/Li-SnO ₂ /Perovskite/Spiro-OMeTAD/Au | 14.78 | [129] |
| SnO ₂ (water treatment) | ITO/SnO ₂ /Perovskite/Spiro-OMeTAD/Au | 18.36 | [130] |
| EDTA-SnO ₂ | ITO/EDTA-SnO ₂ /FA _{0.95} Cs _{0.05} PbI ₃ /Spiro-OMeTAD/Au | 18.28 | [132] |
| SnO ₂ -Graphene | ITO/SnO ₂ -Graphene/C ₆₀ -SAM/Perovskite/Spiro-OMeTAD/Au | 13.36 | [137] |
| N ₂ Plasma-SnO ₂ | ITO/SnO ₂ /Perovskite/Spiro-OMeTAD/Au | 18.10 | [133] |
| SnO ₂ QDs | ITO/SnO ₂ QDs/Perovskite/Spiro-OMeTAD/Au | 17.7 | [146] |
| SnO ₂ | ITO/SnO ₂ /Perovskite/Spiro-OMeTAD/Au | 19.51 | [134] |
| SnO ₂ | ITO/SnO ₂ /CPTA/Perovskite/Spiro-OMeTAD/Au | 18.36 | [136] |
| SnO ₂ (hydrothermal treatment) | ITO/SnO ₂ /Perovskite/Spiro-OMeTAD/Au | 17.3 | [131] |
| SnO ₂ (grown on UVO treated ITO) | ITO/SnO ₂ /Perovskite/Spiro-OMeTAD/Au | 17.5 | [135] |
| SnO ₂ | ITO/SnO ₂ /KCl/Perovskite/Spiro-OMeTAD/Ag | 18.53 | [138] |
| SnO ₂ | ITO/SnO ₂ /HfO ₂ /Perovskite/Spiro-OMeTAD/Au | 19.11 | [147] |
| SnO ₂ | ITO/SnO ₂ /Perovskite-fluorographene QDs/Spiro-OMeTAD/Au | 20.4 | [80] |
| SnO ₂ | ITO/SnO ₂ /Perovskite/Carbon | 11.53 | [148] |
| PEALD-TiO ₂ | ITO/PEALD-TiO ₂ /Perovskite/Spiro-OMeTAD/Ag | 12.2 | [28] |
| PEALD-TiO ₂ /UV-Irradiated TiO ₂ scaffold | ITO/PEALD-TiO ₂ /TiO ₂ scaffold/Perovskite/Spiro-OMeTAD/Au | 8.4 | [120] |
| Electron-beam TiO ₂ | ITO/TiO ₂ /Perovskite/PTAA/Au | 13.5 | [119] |
| Mesoporous TiO ₂ | ITO/TiO ₂ /Perovskite/Spiro-OMeTAD/Au | 12.3 | [149] |
| Magnetron sputtered TiO ₂ | ITO/TiO ₂ /Perovskite/Spiro-OMeTAD/Au | 15.07 | [118] |
| Nb doped TiO ₂ | ITO/TiO ₂ /Perovskite/Spiro-OMeTAD/Au | 16.01 | [150] |
| PEALD-TiO ₂ | ITO/TiO ₂ /PCBM/MAPbI ₃ /Spiro-OMeTAD/Au | 17.70 | [125] |
| TiO ₂ | ITO/TiO ₂ /C ₆₀ /Perovskite/Spiro-OMeTAD/Ag | 16.39 | [126] |
| TiO ₂ | ITO/C ₆₀ /TiO ₂ /Perovskite/Spiro-OMeTAD/Au | 14.74 | [151] |
| TiO ₂ | ITO/TiO ₂ /TiO ₂ nanopillar arrays/Perovskite/Spiro-OMeTAD/Au | 13.33 | [152] |
| None | ITO/Perovskite/Spiro-OMeTAD/Au | 12.70 | [143] |
| Ironic-liquids | ITO/Ironic-liquids/Perovskite/Spiro-OMeTAD/Au | 16.09 | [139] |
| Ti-MOF | ITO/Ti-MOF/Perovskite/Spiro-OMeTAD/Au | 17.43 | [140] |
| Compact C ₆₀ / C ₆₀ nanoparticles | ITO/c-C ₆₀ /C ₆₀ NPs/Perovskite/Spiro-OMeTAD/Au | 17.28 | [141] |
| SnS ₂ | ITO/SnS ₂ /Perovskite/MAPbI ₃ /Spiro-OMeTAD/Au | 13.2 | [142] |

PCE of 8.4%. The prepared photovoltaic module with an area of 8 cm² showed a best efficiency of 4.3% [120].

The photovoltaic devices based on TiO₂ transport layers usually have serious hysteresis behavior due to the deep trap states at TiO₂/perovskite interfaces [121,122]. In addition, the inferior electron extraction performance would lead to the charge accumulation at the interface, which degrades the photovoltaic performance and long-term stability of the devices [123]. The photocatalytic effect of TiO₂ could also lead to device degradation under light illumination due to the introduction of deep traps on the TiO₂ surface [124]. Thus, it is necessary to introduce an interfacial layer to passivate these traps and facilitate electron extraction. Various interfacial materials have been exploited. For example, Kim et al. coated PC₆₀BM on a PEALD-deposited TiO₂ to passivate the traps and improve the electron extraction, which alleviate the hysteresis significantly [125]. As a result, the highest efficiency achieved was improved to 17.70%. In addition, C₆₀ was used as an interfacial layer to improve the TiO₂/

perovskite interface property [126]. C₆₀ is much cheaper than PC₆₀BM while exhibits higher electron mobility. FPSCs with C₆₀ modification demonstrated a best efficiency of 16.39%. Besides the introduction of interfacial layers, oxygen plasma treatment of TiO₂ surface to remove the organic residuals and passivate the oxygen vacancy is also a feasible approach to improve the device performance [127].

SnO₂

SnO₂ is a highly competitive alternative to TiO₂ as an ETL in PSCs. SnO₂ has a deeper conduction band and a higher electron mobility compared with TiO₂ [128]. It can be easily processed by solution methods at low temperature. In addition, it is more stable under sun light illumination. The investigations on SnO₂ as ETLs are mainly focusing on how to improve the conductivity and mobility and modify the conduction band to enhance electron extraction and

Table 5

The photovoltaic performance of FPSCs based on different HTLs processed at low temperature.

| HTL | Device structure | PCE (%) | Ref. |
|--------------------------------------------|--------------------------------------------------------------------------------------|---------|-------|
| NiO _x NCs | ITO/NiO _x NC/MAPbI ₃ /C ₆₀ /Bis-C ₆₀ /Ag | 14.53 | [154] |
| NiO _x NCs | ITO/NiO _x NC/MAPbI ₃ /PCBM/Ag | 13.43 | [155] |
| Cu:NiO _x NPs | ITO/Cu:NiO _x NPs/MAPbI ₃ /PCBM/BCP/Ag | 15.01 | [156] |
| Au:Ni _x O | ITO/Au:Ni _x O/MAPbI ₃ /PCBM/PEI/Ag | 15.9 | [159] |
| NiO _x NPs | ITO/NiO _x NP/Perovskite/PCBM/ZnO NP/Al | 16.1 | [163] |
| NiO _x nanopillar arrays (NAPAs) | ITO/NiO _x /NiO _x NAPAs/Perovskite/PCBM/BCP/Ag | 17.23 | [160] |
| NiO _x | ITO/NiO _x /F2HCNQ/Perovskite/PCBM/BCP/Ag | 20.01 | [157] |
| PhNa-1T | ITO/PhNa-1T/Perovskite/PCBM/Ag | 14.7 | [161] |
| CzPAF-TPA | ITO/CzPAF/MAPbI ₃ /PCBM/ZnO/Al | 12.46 | [162] |
| P(NDI2DT-TTCN) | ITO/P(NDI2DT-TTCN)/Perovskite/PCBM/Ag | 17.0 | [164] |
| BTF6 | ITO/BTF6/Perovskite/C60/BCP/Ag | 18.10 | [165] |

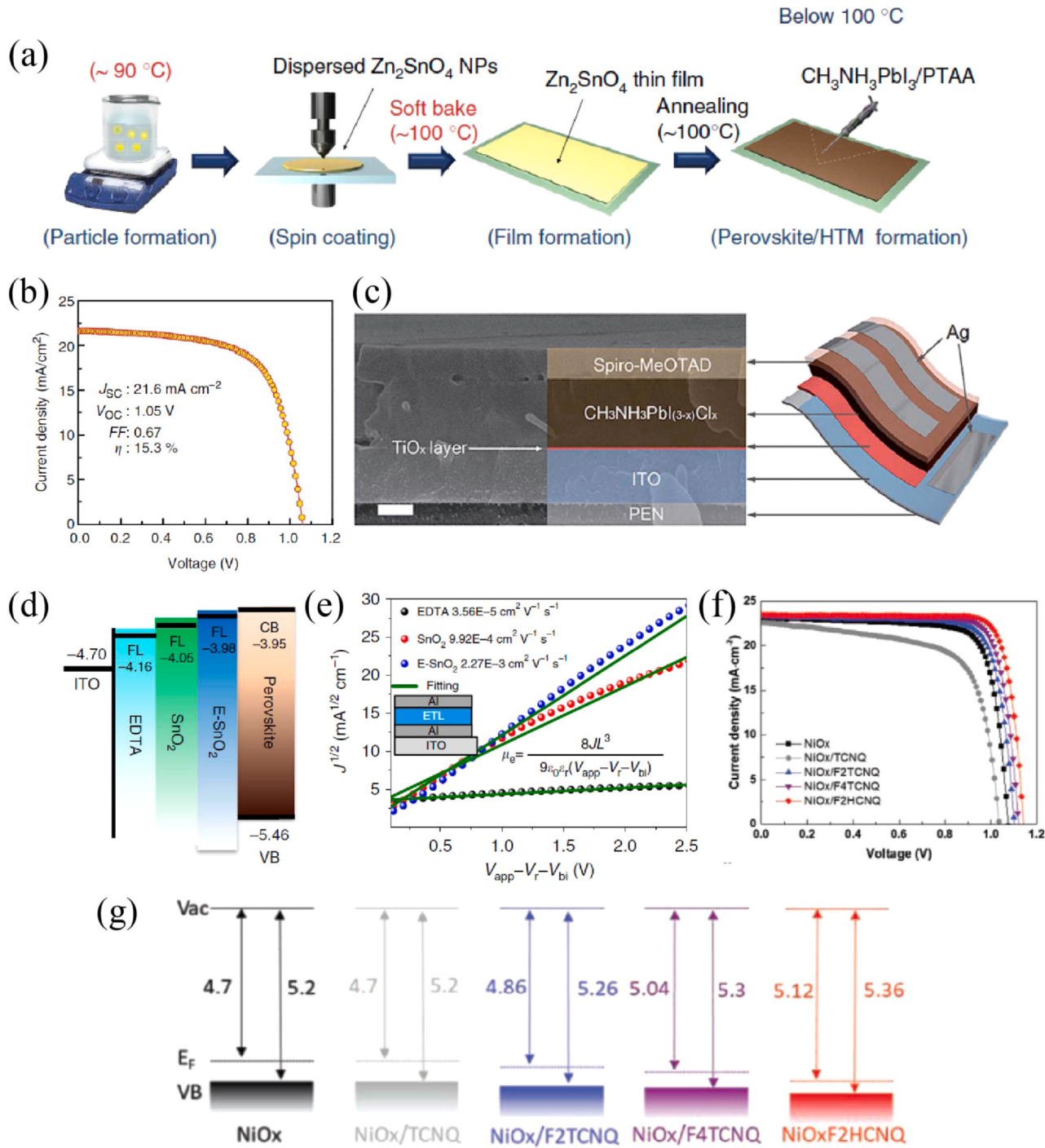


Fig. 7. a) Schematic illustration of the low-temperature process for fabricating flexible devices with Zn_2SnO_4 nanoparticles. b) J-V curve of a FPSC based on Zn_2SnO_4 nanoparticles with a PCE of 15.3% [113]. c) Cross-sectional SEM image of a FPSC based on atomic layer deposited TiO_x layer. d) Schematic illustration of Fermi level of EDTA, SnO_2 , and E- SnO_2 relative to the conduction band of the perovskite layer. e) Electron mobility for EDTA, SnO_2 , and E- SnO_2 using SCLC model, and the inset shows the device structure of ITO/Al/ETL/Al [132]. f) J-V curves of the FPSCs without and with TCNQ, F2TCNQ, F4TCNQ, and F2HCNQ. The best efficiency is 20.01% for FPSCs with F2HCNQ. g) Schematic energy level diagram of NiO_x films without and with TCNQ, F2TCNQ, F4TCNQ, and F2HCNQ.

Part (c) Reprinted with permission from [28]. Copyright 2015, Royal Society of Chemistry. Part (g) Reprinted with permission from [157]. Copyright 2020, John Wiley & Sons, Inc.

transport in FPSCs. Park et al. used Li-doped SnO_2 as an ETL to prepare FPSCs with the highest efficiency of 14.78% [129]. Li-doping could lower the conduction band and increase the conductivity of SnO_2 layers, which will facilitate electron extraction and transport. Wang et al. employed water vapor treated PEALD SnO_2 as ETLs to improve the photovoltaic performance of FPSCs [130]. It was found that the water vapor treatment at $100^\circ C$ can improve the electrical conductivity and mobility of SnO_2 because annealing with water

vapor can facilitate the complete reaction of organic materials and the formation of pure SnO_2 . Based on this technique, efficiency up to 18.36% was achieved in the devices. Liu et al. reported a similar strategy to improve the quality of SnO_2 by hydrothermally annealing the SnO_2 layers [131].

Yang et al. used ethylene diamine tetraacetic acid (EDTA) treatment to adjust the fermi level of SnO_2 to better match with the conduction band of perovskite (Fig. 7d) [132]. In addition, the

electron mobility was three times enhanced (Fig. 7e). The EDTA-SnO₂ enabled the FPSCs with a best efficiency of 18.28%. Subbiah et al. reported a room-temperature processed SnO₂ assisted by low power N₂ plasma treatment in FPSCs [133]. The N₂ plasma could break the alkoxy and hydroxy groups and enable the formation of a metal-oxide-metal network. The fabricated FPSCs demonstrated a champion efficiency of 18.1%. Huang et al. precisely controlled the deposition of SnO₂ layers on flexible substrates by adjusting the solution concentration to form SnO₂ layers with full coverage [134]. The best efficiency of FPSCs was boosted to 19.51%. Dong et al. used ultraviolet ozone (UVO) to treat substrates with an introduction of a trace amount of water on the surfaces [135]. The water could facilitate the growth of SnO₂ films with full coverage and desirable crystallinity by balancing the hydrolysis condensation reaction. The resultant FPSCs exhibited a champion PCE of 17.5%.

Zhong et al. used C₆₀ pyrrolidine tris-acid (CPTA) as an interfacial layer between SnO₂ and perovskite layers [136]. The efficiency was enhanced due to the suppressed recombination of carriers and efficient electron extraction. Besides, graphene nanosheets and KCl were also explored as interfacial layers between SnO₂ and perovskite to improve the photovoltaic performance of FPSCs thanks to the improved charge extraction [137,138].

Other ETLs

Besides the conventional ETLs, some new ETLs have been prepared at low temperature for FPSCs. For example, ionic liquids were employed as ETLs in FPSCs [139]. The ionic liquids have large electrical conductivity, high carrier mobility and suitable work function. The resultant FPSCs exhibited a best PCE of 16.09%. Ryu et al. reported an ETL prepared by crystalline Ti-based metal-organic framework (nTi-MOF) particles with 6 nm in diameter [140]. The combination of well-dispersed nTi-MOF particles and PCBM as ETLs enabled FPSCs with a champion efficiency of 17.43%. Zhao et al. used C₆₀ nanoparticles as a scaffold on C₆₀ compact layer to improve the electron extraction from perovskite layers [141]. The C₆₀ scaffold also enabled the formation of perovskite layers with full coverage. Chu et al. firstly used vacuum deposited SnS₂ as ETL to prepare FPSCs and obtained an efficiency of 13.2% [142]. So far, the efficiencies of FPSCs based on the new ETLs are much lower than those of flexible devices with conventional ETLs, whereas the new ETLs usually own promising stability. Moreover, ETL-free FPSCs have been reported and the best PCE could reach 12.70% [143]. Although the devices could work due to the electron extraction by internal electric field, the efficiency was highly compromised.

Hole transport layers

In FPSCs with p-i-n structures, organic HTLs, such as PEDOT:PSS and PTAA, could be deposited at low temperature, which is compatible with the flexible substrates. However, the stability of organic HTLs is usually poor, which makes the resultant FPSCs unstable in ambient [153]. Hence, much efforts have been devoted to preparing high-quality inorganic HTLs at low temperatures. So far, the mostly used inorganic HTL in inverted FPSCs is NiO_x. Employment of pre-synthesized nanocrystals could be a feasible method to avoid the requirement of high temperature sintering for inorganic materials. Zhang et al. synthesized NiO_x nanocrystals (NCs) with 4 nm in diameter by a chemical precipitation method [154]. The crystalline NiO_x NCs could be easily dispersed in deionized water and spin-coated on flexible substrates without thermal annealing. The nanostructured surface of NiO_x films provides a large interfacial area with perovskite films, making hole extraction more efficient. The resultant FPSCs demonstrated a best efficiency of 14.53% with high air stability. A similar strategy was also reported by Yin et al. [155]. The relatively low conductivity of intrinsic NiO_x hinders the improvement of

NiO_x-based FPSCs. He et al. employed Cu doping to improve the conductivity of NiO_x nanoparticles [156]. The FPSCs based on Cu-doped NiO_x demonstrated a high efficiency of 16.96% and 15.01% for active areas of 0.10 and 1.08 cm², respectively. Ru et al. introduced 3,6-difluoro-2,5,7,8-hexacyanoquinodimethane (F2HCNQ) into a NiO_x NC precursor [157]. The prepared NiO_x films demonstrated improved conductivity by more than ten times and consequently the hole extraction capacity was enhanced by five times. The prepared FPSCs achieved a higher efficiency of 20.01% (Fig. 7g).

Sol-gel NiO_x films usually require a high sintering temperature (~500 °C) to remove the organic materials and get fully crystallized, which is incompatible with flexible substrates that cannot sustain such a high temperature [158]. Hou et al. introduced Au metal into NiO_x precursor films to induce crystallization process at 100 °C [159]. FPSCs based on low-temperature sintered sol-gel NiO_x with Au nanoislands exhibited a PCE of 15.9%. The efficiency could be maintained for more than 1200 h at 65 °C with a humidity of 65%.

Cong et al. prepared nickel oxide nanopillar arrays (NiO_x NaPAs) on flexible substrates by using glancing angle deposition (GLAD) at room temperature [160]. This morphology could enhance the light transmittance of NiO_x films and facilitate the growth of perovskite films with large grains. The FPSCs based on NiO_x NaPAs showed a high PCE of 17.23%. Beside the conventional NiO_x, some new hole transport materials are also synthesized to prepare FPSCs, such as PhNa-1T and CzPAF-TPA, while the resultant efficiency is relatively low [161,162]. Yu et al. designed a new small molecule D-A-D-type HTM (BT6) by making dicyanofluoranthene as the key intermediate to prepare high efficiency inverted FPSCs. The matched energy level with perovskite and superior hole mobility enabled BT6-based FPSCs to show an efficiency of 18.10%.

Effect of charge transport layers on the mechanical flexibility of devices

Generally, the commonly used organic transport layers, such as PEDOT:PSS, PTAA, PCBM, Spiro-OMeTAD, are more mechanically flexible than ITO and perovskite films due to the lower Young's modulus. For inorganic transport layers, these layers with nanoparticle or nanocrystal structures also have better mechanical tolerance [166,167]. Therefore, the mechanical property of pure charge transport layers (CTLs) is not the obstacle in the bending operation of FPSCs currently. However, the adhesive property between CTLs and perovskite films and the release of strain by CTLs play a critical role on the mechanical flexibility of FPSCs [168–170]. PC₆BM ETL has been considered to have poor adhesion with perovskite films, which leads to performance degradation in bending tests of FPSCs [169]. Huang et al. employed a novel glued poly(ethylene-co-vinyl acetate) (EVA) as an interfacial layer between PCBM and perovskite layers to enhance the adhesion. The fabricated FPSCs could retained over 85% of initial PCE after 5000 bending cycles at a radius of 2.5 mm [171]. A polyethyleneimine (PEI) layer is introduced as an interfacial layer between perovskite and Spiro-OMeTAD layers to improve the mechanical flexibility of the devices owing to enhanced adhesion [172].

CTLs with special structures have been designed to release stress in FPSCs. Hu et al. used a polystyrene-doped nanocellular PEDOT:PSS (NC-PEDOT:PSS) as a HTL to release stress in FPSCs. The perovskite films deposited on NC-PEDOT:PSS films demonstrate much better mechanical flexibility than the counterparts deposited on PEDOT:PSS (Fig. 8a–c) [173]. The enhanced mechanical flexibility is due to the soft nanocellular scaffold of NC-PEDOT:PSS that can release stress and avoid fractures. Meng et al. reported a vertebrae bionics design with a structure of ITO/PEDOT:EVA/perovskite to improve the mechanical flexibility of perovskite films and FPSCs (Fig. 8d and e). The interfacial layer of PEDOT:EVA effectively absorbs and releases stress due to the strong adhesion with ITO and perovskite layers and the vertebral structure [17].

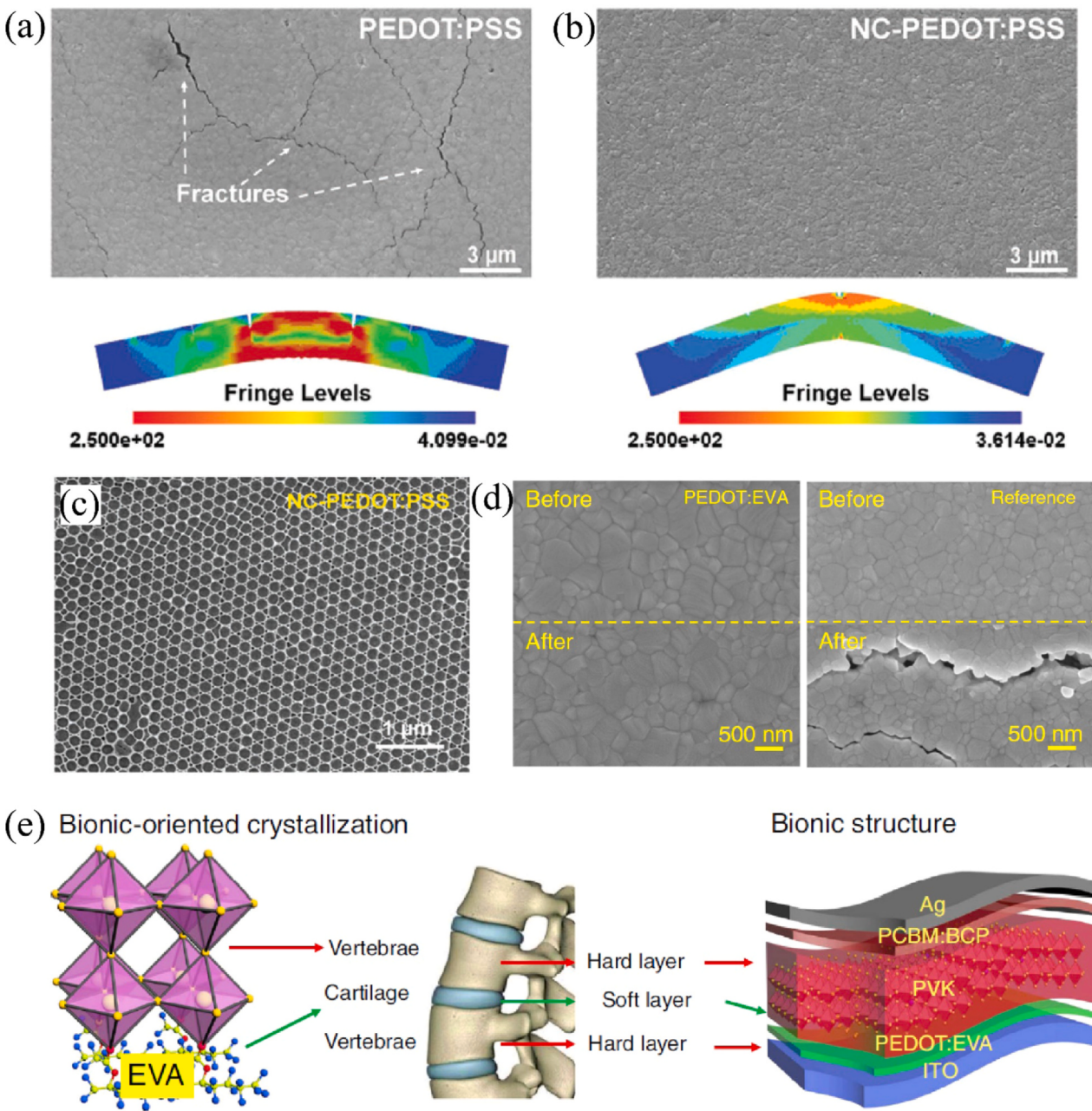


Fig. 8. SEM images and finite-element simulation of flexible perovskite films based on a) PEDOT:PSS and b) NC-PEDOT:OSS under bending. c) SEM image of NC-PEDOT:PSS layer [173]. d) SEM images of perovskite films deposited on PEDOT:EVA and PEDOT films before and after bending. e) Biomimetic mechanisms of the vertebrae and FPSCs [17].

The displacement of CTls with perovskite films and substrates is detrimental to the photovoltaic performance and mechanical flexibility of FPSCs under bending operation. Hence, enhancing the adhesion between CTls and perovskite is necessary. To design and synthesize novel flexible CTls with good adhesion on both substrate and perovskite surfaces is a possible way to further improve the mechanical flexibility of FPSCs. So far, few works are focusing on those issues. More efforts are thus needed to explore new functional materials and novel structures specifically for FPSCs.

Preparation of high-quality perovskite films on flexible substrates

The low thermal resistance of flexible substrates can influence the fabrication of high-quality perovskite films. Normally, the obtained perovskite films demonstrate large variation in quality

compared with counterparts prepared on glass substrates using the same fabrication methods. Hence, several specific techniques have been explored to achieve high-quality perovskites (organic-inorganic hybrid, inorganic and lead-free perovskites) on flexible substrates and improve the efficiency and mechanical durability of FPSCs.

Low-temperature processing methods

Several strategies have been developed for the preparation of high-quality perovskite films at room temperature. For instance, Jeon et al. developed a laser crystallization method to prepare perovskite films at room temperature (Fig. 9a) [174]. The absorption of near-infrared laser ($\lambda = 1064$ nm) by ITO and PEDOT:PSS layers induces photo-thermal heating, which leads to the crystallization of perovskite films. The resultant PSCs based on MAPbI₃ demonstrate

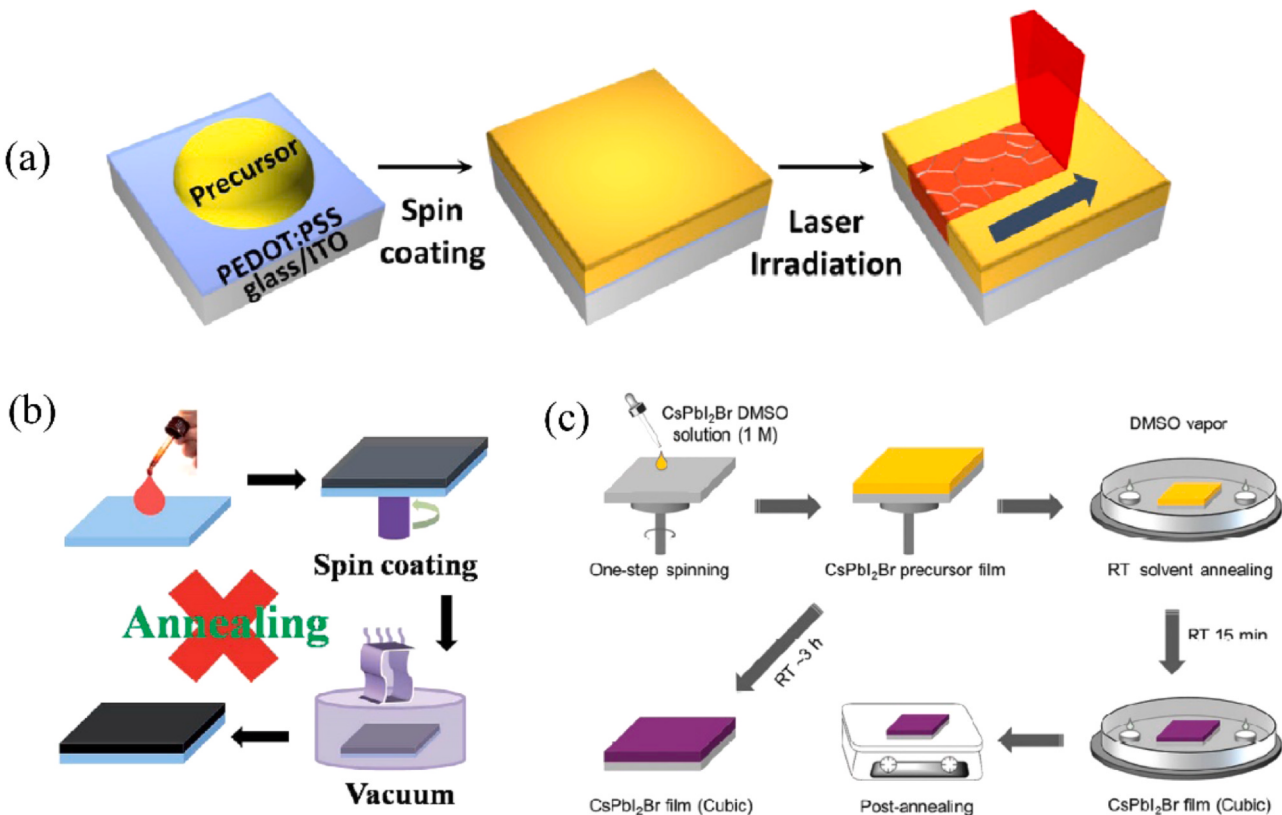


Fig. 9. a) Schematic description of perovskite film formation process by laser annealing. Precursor solution is spread onto PEDOT:PSS coated glass/ITO substrate. Thin-film is formed by spin-coating. Then, the film is exposed to laser beam scan. b) Schematic diagram of the vacuum-assisted drying approach to deposit the all-inorganic perovskite films. c) Schematic diagram of preparation procedures of the CsPbI₂Br films with room temperature vapor annealing and direct thermal annealing, respectively. Part (a) Reprinted with permission from [174]. Copyright 2016, American Chemical Society. Part (b) Reprinted with permission from [177]. Copyright 2018, Royal Society of Chemistry. Part (c) Reprinted with permission from [178]. Copyright 2018, John Wiley & Sons, Inc.

PCEs of 11.3% and 8.0% based on glass and PET substrates, respectively. Recently, our group used another laser annealing method to prepare high-performance PSCs at room temperature based on a different principle [175]. The wavelength of laser beam was changed to visible range, which can induce photo-thermal heating inside perovskite films. The temperature gradient generated in the perovskite films owing to different light absorption coefficients in crystalline and amorphous regions can accelerate the crystallization of perovskite films with enlarged grain sizes. The prepared mixed-cations PSCs demonstrate a best efficiency of 21.50% under optimized laser annealing with a wavelength of 450 nm. Lei et al. explored vacuum deposition method to prepare HTL and perovskite films, which enabled FPSCs to have efficiencies up to 19.23% with a small area and 13.0% with an active area of 16.0 cm². However, the formed perovskite films need post-annealing at 100 °C to further improve their crystallization [176].

Hu et al. used a vacuum-assisted drying process to prepare inorganic perovskite films at room temperature, which usually requires a high annealing temperature of 310 °C (Fig. 9b) [177]. By adjusting the ratio of Dimethylformamide (DMF) and DMSO, high-quality CsPb_{0.96}Bi_{0.04}I₃ perovskite films were successfully crystallized via a vacuum-assisted dry process. The FPSCs based on the inorganic perovskites exhibited a champion PCE of 11.47%. Rao et al. reported room-temperature DMSO annealing treatment for inorganic CsPbI₂Br perovskite films (Fig. 9c) [178]. However, rigid devices show a maximum PCE of only 6.4% and the efficiency was further enhanced to 10.4% by post-annealing the treated perovskite films at 120 °C. FPSCs based on the perovskite films prepared under the same conditions demonstrate a champion PCE of 7.3%. Xi et al. evaporated SnI₂ layers on the FAI/polymer layers to create uniform lead-free

FASnI₃ films while the fabricated lead-free FPSCs demonstrate the best efficiency of 3.12% only [179]. In summary, although the aforementioned strategies can enable the successful fabrication of FPSCs without thermal annealing, the obtained efficiencies are relatively low in comparison with those of the thermal annealed PSCs due to the poor quality of the room-temperature processed perovskite films.

Composition and additive engineering

Composition tailoring and additive introductions are highly effective strategies for improving the quality of perovskite films prepared at low temperatures [180]. Bi et al. found that the morphology and optoelectronic properties of perovskite films grown on flexible substrates can be improved by tuning the perovskite precursor ratio (FAI/MABr) (Fig. 10a and b) and resultant FPSCs under optimized preparation conditions demonstrate a best efficiency of 18.1% [181]. Feng et al. employed dimethyl sulfide (DS) as an additive to control the growth of perovskite films deposited on flexible substrates (Fig. 10c) [31]. Fourier transform infrared spectroscopy revealed that the DS additive can react with Pb²⁺ and form an intermediate phase, which retards the crystallization process. The prepared perovskite films exhibit large grains and low defect densities, leading to an improved PCE of 18.4%. Wu et al. used NMP and MACl as synergistic additives to optimize FAPbI₃ perovskites on flexible substrates [32]. The introduction of NMP could enable the formation of FAI-PbI₂-NMP intermediate, which retards the crystallization process. The employment of MACl could facilitate the phase transition of black perovskites at a low temperature. Based on the synergistic

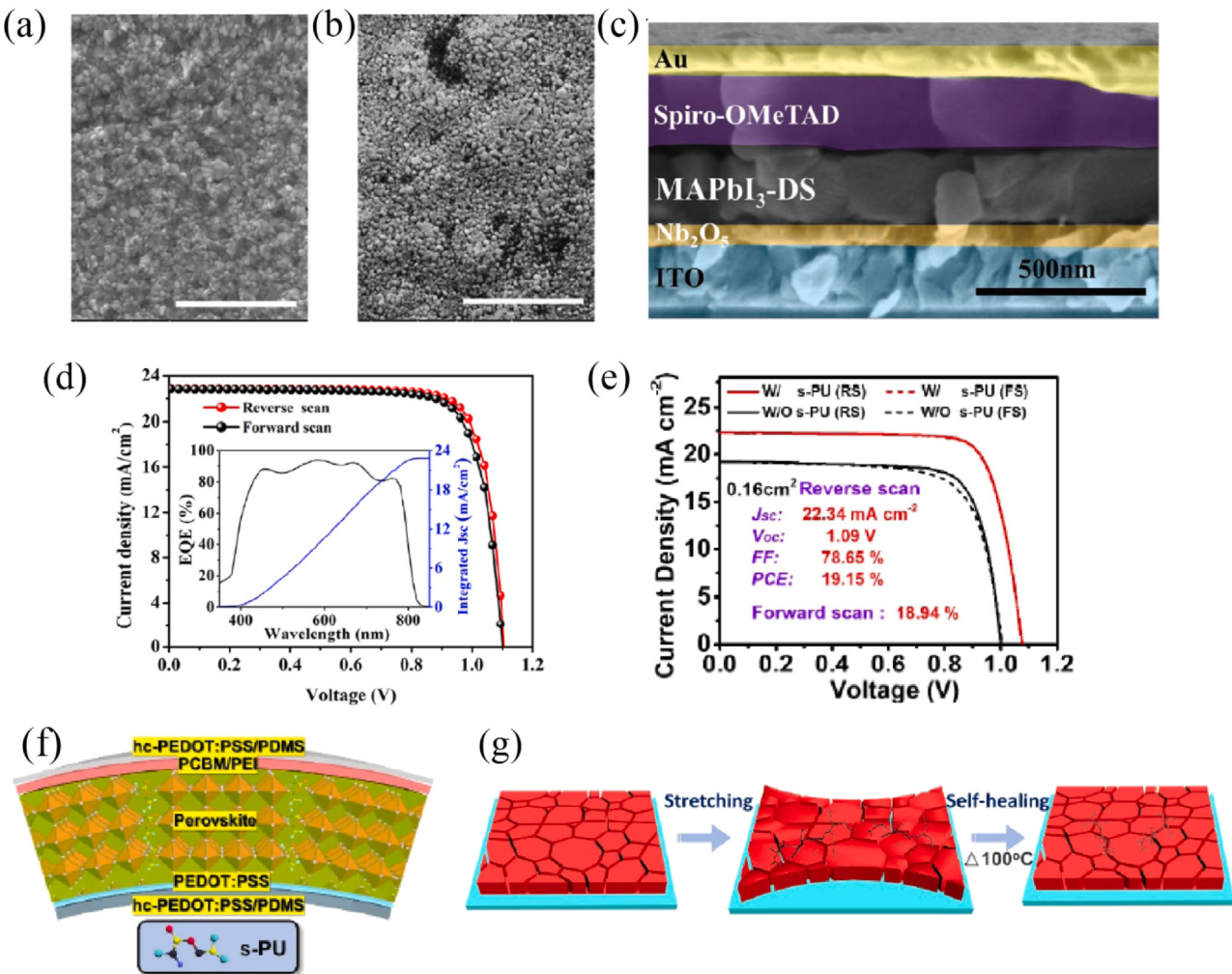


Fig. 10. SEM images of perovskite films on a) ITO/glass and b) ITO/PET substrates. c) Cross-sectional SEM image of a completed flexible device with MAPbI₃-dimethyl sulfide absorber. d) J-V curve of a FPSC based on fluorographene quantum dots modified perovskite layer with a champion PCE of 20.40%. e) J-V curves of stretchable PSCs based on a self-healing polyurethane (s-PU) with a best PCE of 19.15%. f) Device structure of a stretchable PSC. g) The schematic of the mechanically self-healing process for perovskite films. Part (b) Reprinted with permission from [181]. Copyright 2017, John Wiley & Sons, Inc. Part (c) Reprinted with permission from [31]. Copyright 2018, John Wiley & Sons, Inc. Part (d) Reprinted with permission from [80]. Copyright 2020, American Chemical Society. Part (g) Reprinted with permission from [63]. Copyright 2020, John Wiley & Sons, Inc.

improvements, the FAPbI₃-based FPSCs showed the best efficiency of 19.38%.

Yang et al. used exfoliated fluorographene quantum dots to passivate the grain boundaries and surface of perovskite films [80]. The resultant films demonstrate low defect densities and low charge recombination and the FPSCs (n-i-p structure: PEN/ITO/modified SnO₂/perovskite/spiro-OMeTAD/Ag) based on this approach show the efficiency of 20.40%. For inorganic FPSCs, Yang et al. used Al-doped ZnO (AZO) as an ETL and tert-butyl cyanoacetate (t-BCA) as a passivation layer to prepare FPSCs based on inorganic CsPbI₂Br perovskites at a temperature of 120 °C [182]. The employment of AZO layer significantly improved the crystallinity of perovskite films. The defects and charge recombination were highly passivated and suppressed. Consequently, the best efficiency of inorganic FPSCs was improved to 15.08%.

The introduction of additives can also enhance the mechanical flexibility of FPSCs. Huang et al. introduced a novel glued poly(ethylene-co-vinyl acetate) (EVA) as an interfacial layer between perovskite and PCBM films [171]. This glue could enhance the adhesion between perovskite and PCBM layers to improve the bendability of flexible devices. On the other hand, grain boundaries of perovskite films are highly vulnerable under mechanical stress, which deteriorates the deformability and photovoltaic performances

of FPSCs. Li et al. introduced a photo-crosslinked fullerene [6,6]-phenylC₆₁-butyric oxetane dendron ester (C-PCBOD) into grain boundaries of perovskite films to enhance the mechanical durability [183]. The soft C-PCBOD could buffer the compression of perovskite grains under mechanical stress and the obtained FPSCs demonstrate a high PCE of 18.1% with enhanced bending stability.

Meng et al. incorporated a self-healing polyurethane (s-PU) with dynamic oxime-carbamate bonds in the grain boundaries of perovskite films (Fig. 10e) [63]. The s-PU could release the mechanical strain and repair cracks at the grain boundaries, which significantly improved the stretchability and deformability of perovskite films (Fig. 10f). The prepared FPSCs could recover 88% of initial PCEs after 1000 cycles at 20% stretching. In addition, due to the defect passivation of s-PU at the grain boundaries, the stretchable FPSCs exhibited a best efficiency of 19.15% (Fig. 10g). Liu et al. used PMMA-CNTs composite as an additive to facilitate charge transport (due to high mobility of CNTs) and passivate defects (due to the interaction between Lewis-base -COOH group of PMMA and Pb²⁺ at grain boundaries of perovskite films) at grain boundaries in perovskite films. The prepared FPSCs with PMMA-CNTs additives demonstrated an impressive PCE of 18.3% with superior mechanical flexibility [184]. An additive of trimethyltrivinyl-cyclotrisiloxane (V3D3) was introduced at grain boundaries (GBs) in perovskite films to in situ

cross-link GBs. The prepared FPSCs demonstrates a champion efficiency of 20.0% [59]. Yang et al. used artemisinin to passivated the uncoordinated Pb^{2+} ions, which effectively reduced the perovskite film's trap density. The prepared FPSCs demonstrated a record efficiency of 21.10% [33].

Toward commercialization

The relatively low cost and high efficiency of PSCs are two merits which promise the viable commercialization in the future [185]. It is estimated that the whole material cost for perovskite solar module is about US\$20 per square meter. Another critical factor in cost reduction is the low manufacturing cost by solution process, such as R2R method. The cost of manufacturing lines for PSCs are around one-third of those for commercial multicrystalline silicon solar cells. Therefore, the total cost of PSCs is about US\$40 per square meter, which is 50% lower than that for silicon solar cells (US\$80) [186]. FPSCs should be the foremost commercialization option because they are expected to be fabricated by R2R mass production at low cost. In addition, flexible devices could fulfill the highly diverse applications, such as wearable and portable electronics, unmanned systems, smart buildings, and aerospace applications [20,74,187]. In practice, although the efficiency of FPSCs with small area is relatively high, the fabrication of large-area FPSC or flexible modules with high efficiency and stability is still at an early stage. Notably, long-term stability should be ensured by exploring efficient encapsulation techniques.

Large-area fabrication by R2R method

Fabrication techniques for small area devices, such as spin-coating and physical vapor deposition, are incompatible with low-cost and high-speed mass production [188,189]. Currently, R2R method may be the most promising strategy for upscaling the fabrication of PSCs and promoting commercialization, like its successful application in the mass production of organic solar cells. Investigations on R2R method integrated with slot die coating, blade coating, solution shearing coating, spray coating and gravure-printing have been focusing on the deposition parameters for each layer on large scale to ensure the superior morphologies and qualities, the use of nontoxic solvents, and the optimization of photovoltaic performance.

Controlling the growth of perovskite films at a fast speed with high quality is key to the photovoltaic performance of R2R processed flexible devices because the substrates always keep moving. It has been found that the deposition of perovskite films is sensitive to the substrates during R2R processes. Schmidt et al. reported successful one-step preparation of perovskite films on ITO/PEDOT:PSS substrates while unsuccessful on ITO/ZnO/PCBM substrates [190]. Perovskite films can also be prepared with two-step process, whereas the efficiency of flexible devices on ITO/PEDOT:PSS substrates was much lower than that on ITO/ZnO/PCBM substrates.

The typical solvents used in perovskite precursors, such as DMF, N-Methyl-2-pyrrolidone (NMP) and gamma-Butyrolactone (GBL) are not suitable for industrial mass production due to their toxicity. A cosolvent of nontoxic DMSO and 2-butoxyethanol (2BE) were employed to prepare perovskite precursors [191]. By thermal annealing with a fast temperature ramp-up, a uniform $Cs_{0.15}FA_{0.85}PbI_{2.85}Br_{0.15}$ perovskite film was successfully formed by slot die R2R coating (Fig. 11a). The best efficiency obtained was 15.2% for a small area FPSC (0.09 cm^2). The coating process could be formed on substrates with a width of 30 cm and the web speed of $3\text{--}5\text{ m min}^{-1}$, which showed a potential for the future commercialization. Kim et al. used a hot-deposition approach to slot-die coat perovskite films by simply heating up the coating bed to 130°C during fabrication (Fig. 11d and e) [192]. This method speeds up the crystallization of

perovskite and reduces the exposure time to the humid ambient. In addition, the addition of PEO into perovskite precursor could significantly enhance the humidity tolerance of the devices. The best efficiency of the R2R processed FPSCs reaches 11.7% (Fig. 11f).

Bu et al. used slot die coating method to prepare SnO_2 films on rough and soft plastic substrates [40]. Under potassium treatment on SnO_2 surface, the defect density between SnO_2 and perovskite films was significantly suppressed (Fig. 11b). The flexible modules with an area of 30 cm^2 show a best efficiency of 15.22% (Fig. 11c). A self-assembled monolayer (C3-SAM) was coated on PEDOT:PSS to facilitate the following roll coating of perovskite films [193]. The coated perovskite films demonstrated full coverage and smooth surface, which is favorable for the photovoltaic performance of the devices.

Besides the slot die R2R strategy, blade coating has been used to fabricate FPSCs with large area. Dai et al. introduced ammonium chloride (NH_4Cl) into a perovskite precursor to retard the nucleation which prevented voids at the interface between perovskite and substrate [47]. The high-quality perovskite films with low defects enabled flexible perovskite module with a record efficiency of 15.86% and an area of 42.9 cm^2 . Thiourea was explored as an additive in the perovskite precursor to enhance the crystallinity of blade-coated perovskite films [194]. With double HTLs of PEDOT:PSS and PTAA, the blade-coated FPSCs show a best PCE of 19.41% with a high FF of 81% with small area. Other techniques such as solution-shearing and ultrasonic spray-coating methods have also been utilized in the preparation of FPSCs [195–197]. Compared with FPSCs based on single junction, tandem solar cells are supposed to a preferred commercialization choice due to their improved efficiency. Recently, Palmstrom et al. fabricated two terminals all perovskite tandem solar cells with a record PCE of 21.3% on PET substrates, which is much higher than that of single junction counterparts [198].

Recently, Chung et al. achieved an efficiency of 20.75% in FPSCs and a certified PCE of 19.9% by employing a porous planar ETL with a structure of SnO_2 NPs (2 nm) and Zn_2SnO_4 NPs (20 nm) as a compact layer and a porous layer, respectively [43]. The introduction of porous layer of Zn_2SnO_4 could enhance the charge collection due to the better energy alignment and improved surface contact. Moreover, the porous structure could yield a lower surface energy, leading to grain enlargement of as-deposited perovskite films. A large-area flexible sub-module over a $10 \times 10\text{ cm}^2$ area was fabricated by solution-shearing and a laser scribing method. The flexible sub-module with the porous planar structure showed an outstanding PCE of 15.50% and 17.50% with an aperture area of 100 cm^2 and active area of 90 cm^2 , respectively. Additionally, PCEs of 12.9% and 14.3% on an aperture area of 225 cm^2 and an active area of 202.5 cm^2 and PCEs of 11.8% and 13.1% on an aperture area of 400 cm^2 and an active area of 360 cm^2 were obtained, respectively.

In the R2R processing production of FPSCs, the conversion of wet perovskite film of precursor state into intermediate phase has been considered as a critical step [52]. Kim et al. reported a R2R compatible gravure-printing method to successfully prepare high efficiency FPSCs using eco-friendly antisolvent bathing with wide processing window. By integrating with R2R process, the gravure-printed $FAPbI_3$ films demonstrated high crystallinity and uniformity by dipping into a mixed solvent of tBuOH and EA (Fig. 12a). The gravure printed FPSCs exhibited a champion efficiency of 19.1% (Fig. 12b and c). The fully R2R gravure printed FPSCs except metal electrode deposition demonstrated a record efficiency of 13.8% among fully R2R processed FPSCs (Fig. 12d–f). This work significantly promotes the development of large-scale production of FPSCs via low-cost R2R processes.

Device encapsulation

Despite the substantial progress in the efficiency of FPSCs, the intrinsic instability of perovskite materials under water and oxygen

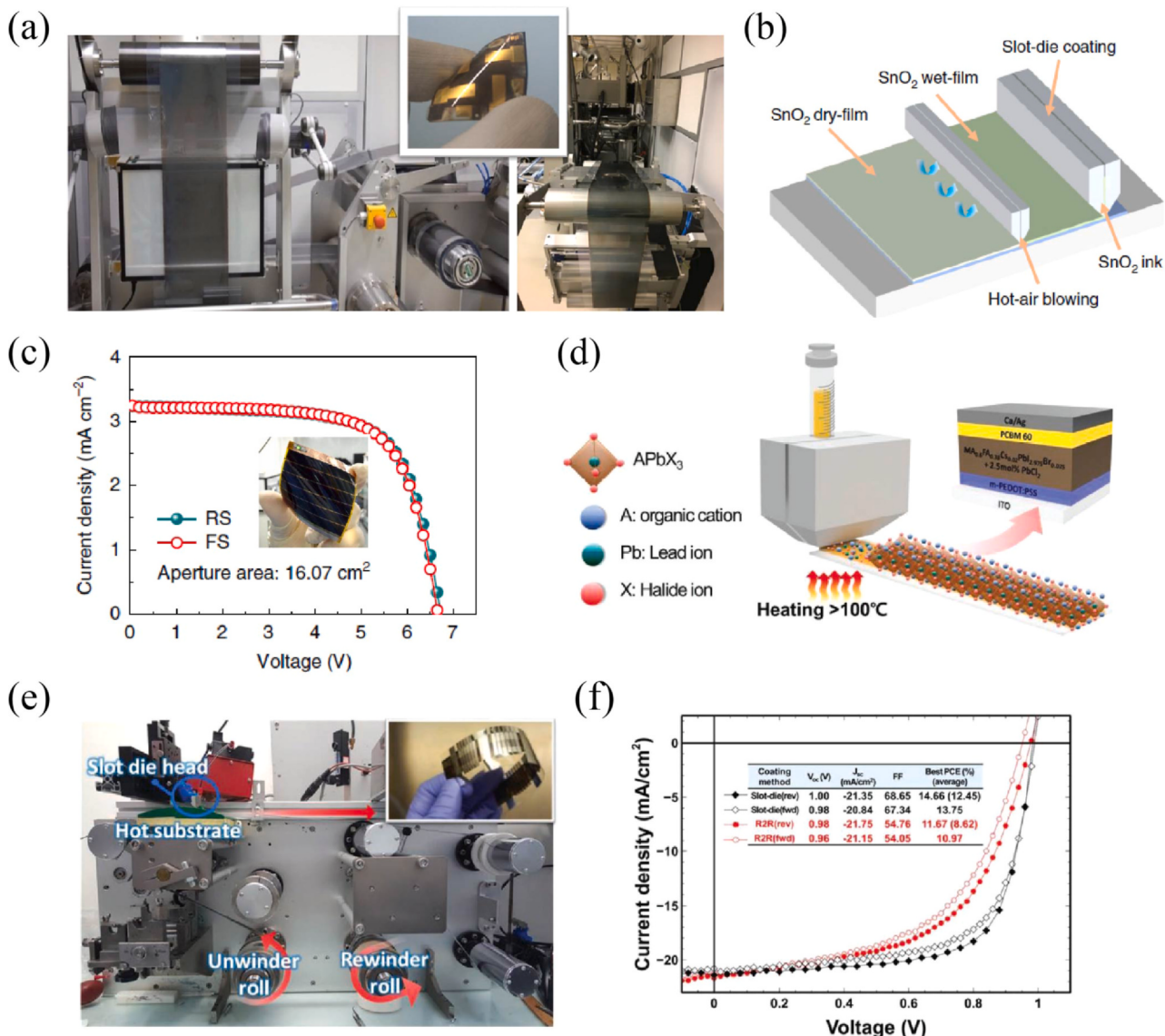


Fig. 11. a) Photograph images of a roll-to-roll coated perovskite layer ($\text{Cs}_{0.15}\text{FA}_{0.85}\text{PbI}_{2.85}\text{Br}_{0.15}$) and an example of the manufactured flexible device. b) The schematic of slot-die coating SnO_2 films. c) J-V curves of a flexible perovskite module based on slot-die coated SnO_2 with a PCE of 15.22%. The inset is a photograph of a complete module [40]. d) Schematic illustration of the device structure and slot-die coating of PSCs with high processing temperature. e) Photo of a slot-die coater equipped a roll to roll machine. f) J-V curves of FPSCs prepared by the roll to roll method.

Part (a) Reprinted with permission from [191]. Copyright 2018, John Wiley & Sons, Inc. Part (f) Reprinted with permission from [192]. Copyright 2019, John Wiley & Sons, Inc.

significantly hinders the commercialization of the devices [199]. Therefore, efficient encapsulation technologies are highly desired to block the ingress of moisture and oxygen to ensure the long-term stability of FPSCs. Plastic barrier materials (Viewbarrier) with 3 M adhesive tapes have been used as encapsulation films to seal FPSCs, which can significantly extend the lifetime of the devices in ambient air [200]. However, some plastic substrates are permeable for water and oxygen. Tavakoli. et al. reported that functional PDMS films with nanocore structure can be attached onto the front surface of flexible substrates to simultaneously enhance the light transmittance and repel water due to the hydrophobic property of PDMS [46]. The polyurethane resin was also employed as encapsulation films to extend the long-term stability of FPSCs [18]. In addition, some novel functional materials like 2D materials can be introduced in the

devices for encapsulation because 2D materials are normally impermeable to air.

Due to the low light and high oxygen-moisture transmittances of polymer substrate with transparent electrode, the efficiency and stability of FPSCs is inferior than rigid counterparts. Recently, Cho et al. employed a plasma-polymerized-fluorocarbon (PPFC) thin film as an antireflection (AR) coating material to simultaneously improve the light transmittance and oxygen-moisture barrier property by depositing PPFC films on PET substrates via a mid-range frequency sputtering process (Fig. 13a) [201]. Due to the very low refractive index (~1.38) of PPFC over a wide wavelength range, these films decrease the average reflectance by 2.22% and increase the average transmittance in the visible light region by 1.40% (Fig. 13b-d). The PCE of FPSCs has been increased from 18.6% to 20.4% by PPFC films

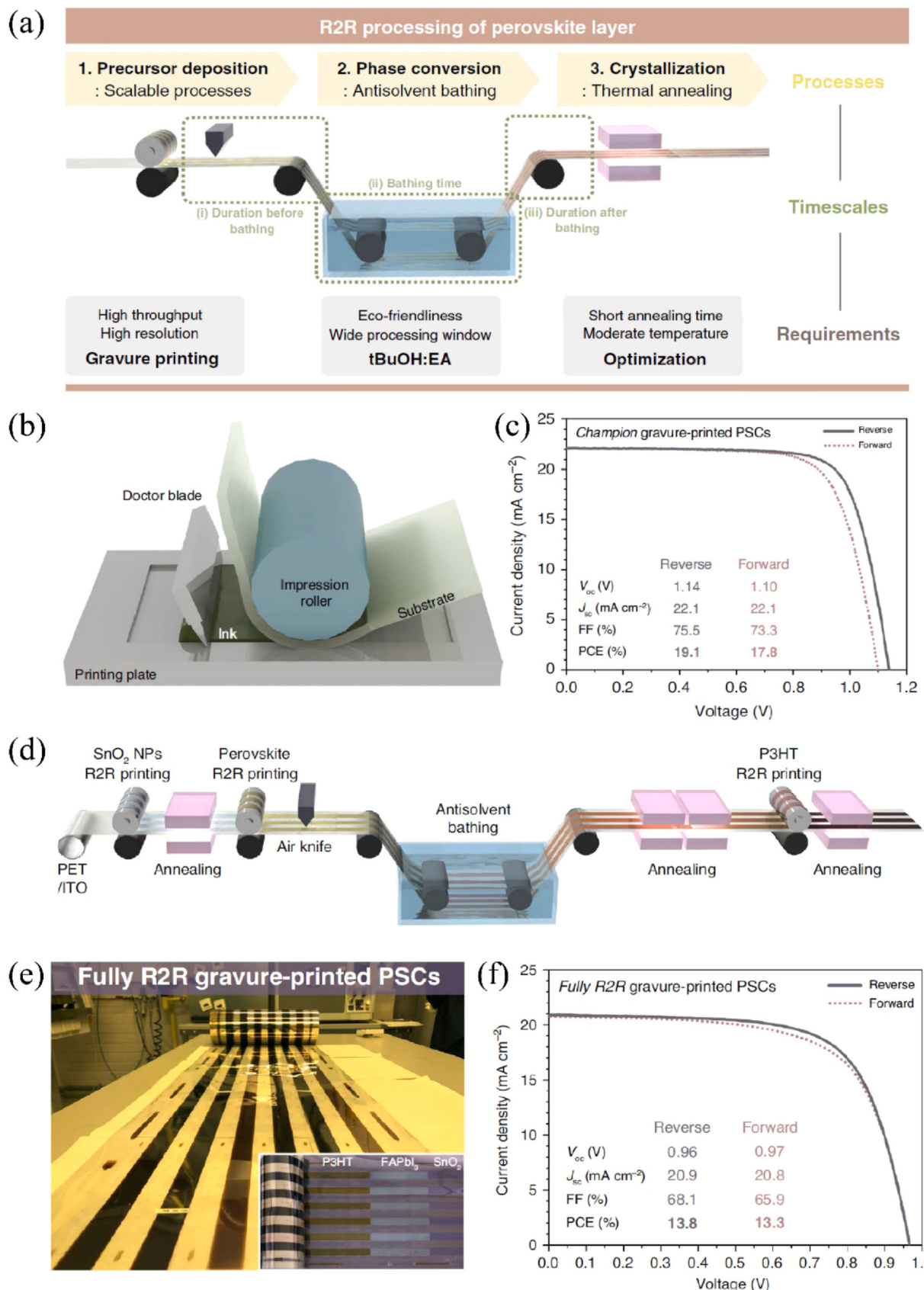


Fig. 12. a) Schematic diagram depicting R2R gravure printing of perovskite layer. b) Schematic illustration of table-top gravure printing. c) A J-V curve of champion device fabricated by gravure-printing. d) Diagram showing R2R processing for the fabrication of FPSCs. e) Photograph of fully R2R processed FPSCs. (insert) Image of a R2R processed roll showing constituent layers after removing each layer manually. f) The J-V curves of fully R2R gravure-printed FPSCs [52].

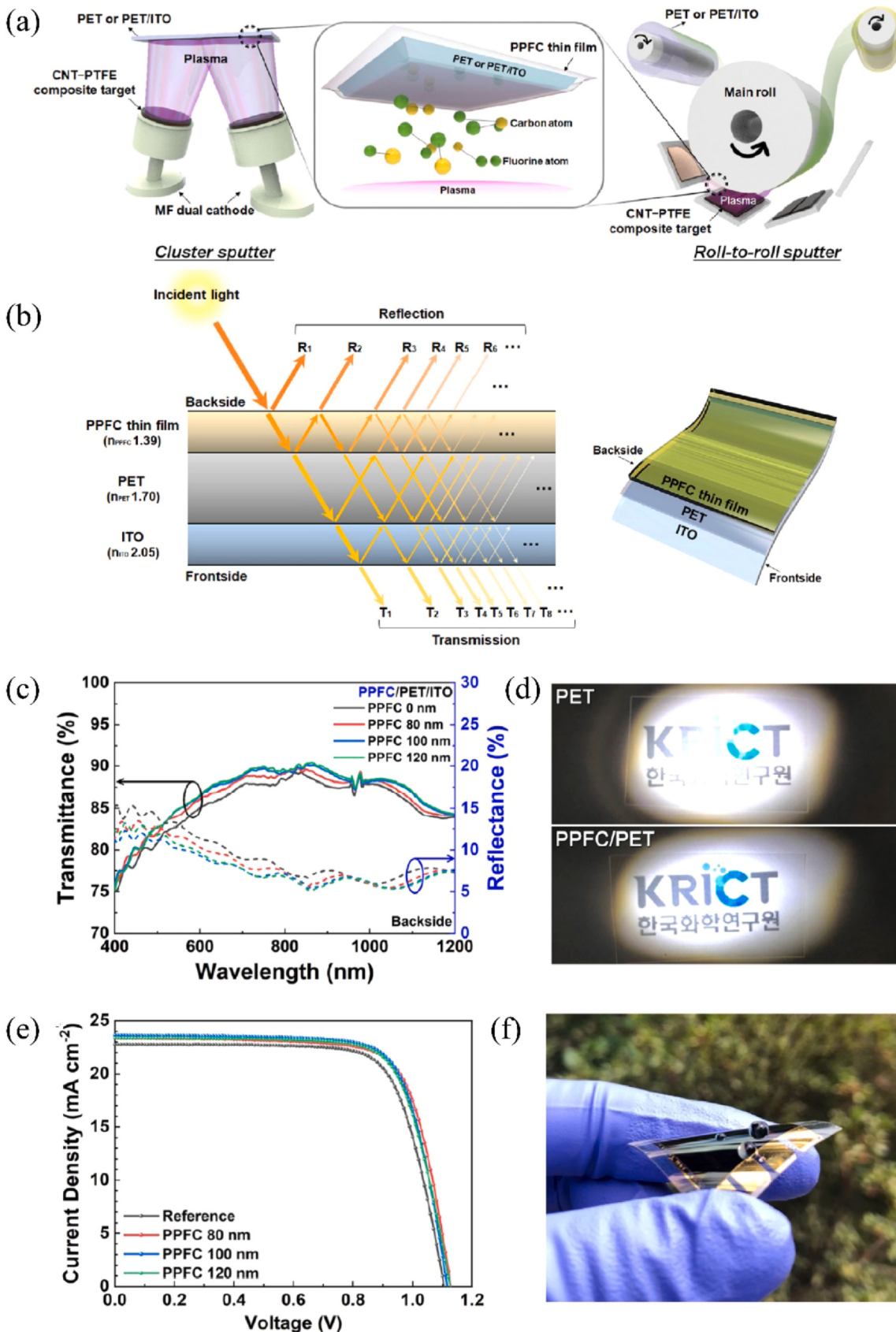


Fig. 13. a) Illustration of the sputtering process to deposit PPFC thin films with cluster and roll-to-roll sputter equipment. b) Principle of antireflection effect in the PPFC/PET/ITO substrate. Transmittance and reflectance spectra on the front and back side of PPFC/PET/ITO with different PPFC coating layer thickness. d) Photograph of the antireflection effect. e) J-V curves of representative solar cells with or without PPFC thin film of different thickness. f) Hydrophobic characteristic of the PPFC thin film. Part (f) Reprinted with permission from [201]. Copyright 2021, Elsevier Ltd.

with optimized thickness (Fig. 13e). Besides, the long-term stability in humid environments has been improved significantly due to the hydrophobic surface of PPFC films (Fig. 13f). This work demonstrates a promising strategy which could simultaneously improve the efficiency and stability of FPSCs.

Conclusion and outlook

In summary, remarkable progress has been achieved in the development of PSCs due to the deeper understanding in chemical and optoelectronic properties of raw materials, fabrication technologies and working mechanisms of devices, which leads to the highest PCE of 25.5% for rigid PSCs and 21.1% (21.3%) for FPSCs (tandem device) so far. For flexible devices, the successful exploration of flexible substrates, transparent electrodes, low temperature processed charge transport layers, and high-quality perovskite films deposited on flexible substrates plays a key role on the fast progress. Besides high efficiency, lightweight and good stretchability are also attractive characteristics of FPSCs being investigated. R2R fabrication of FPSCs has been recognized as a feasible approach for the mass production and commercialization of the devices. Encapsulation strategy for ensuring long-term stability of FPSCs has also been developed though still at an early stage.

Three types of flexible substrates, including flexible glasses, metal foils, and polymer substrates are compared here in terms of light transmittance, thermal and chemical tolerance, mechanical durability, and water and oxygen blocking ability. Flexible glass substrates are relatively expensive and fragility, which are two factors hindering the wide applications. Metal foils, such as Ti foils and Cu foils, can be used as both substrates and electrodes while transparent top electrodes are needed due to their opaque property. Plastic substrates are most popularly used in FPSCs, while the high water and oxygen permeating rate must be considered in achieving long-term stability of FPSCs. Moreover, the commonly used polymer substrates, such as PET and PEN, have relatively poor thermal tolerance and low temperature processing is needed in device fabrication.

For transparent conductive electrodes, silver nanowires, metal grids, carbon nanotubes, graphene, and PEDOT:PSS have been explored to replace ITO electrodes in FPSCs despite the resultant relatively lower efficiencies. Transparent silver nanowires (NWs) electrodes own high conductivity and can be prepared at large scaling by solution process. However, the random deployment of nanowires leads to large roughness of films. The halides in perovskites would chemically react with Ag, leading to device degradations. GO flakes, ITO, AZO and PEDOT:PSS have been coated onto Ag NWs to overcome these issues. For metal grids, the complex techniques and high cost are not suitable for large-area fabrication, which may prevent its wide applications. Graphene-based FPSCs demonstrate high efficiency and superior bendability due to high conductivity and transmittance of graphene electrodes while large-area fabrication could be a limitation of this technique.

For charge transport layers, many efforts have been devoted to the fabrication of ZnO, TiO₂, SnO₂, and NiO_x layers with high quality at low temperature. For devices with a normal structure, SnO₂ may be the best choice for ETL due to the good stability and suitable band structure. NiO_x shows advantages over organic semiconductors as HTLs in an inverted device due to the better stability. To get high-performance FPSCs, composition tailoring and additives engineering of perovskite layers are also essential techniques because the crystallinity, band structure and mechanical property of perovskite layers can dramatically influence the photovoltaic performance of the resultant PSCs under mechanical strain.

In the future development of FPSCs, the exploration of flexible transparent electrodes with high conductivity and transmittance, low-cost and upscaling processability is still urgent for the

commercialization target. For charge transport layers and perovskite layers, large-area fabrication of the films is the main research direction. Although R2R method has already been applied to prepare transport layers and perovskite films, the efficiency of obtained devices is relatively low. More research efforts, such as interface modification and additive introduction, are desired in the fabrication process. Efficient encapsulation methods on both bottom and front surfaces should be further developed to get acceptable long-term stability of FPSCs. In addition, flexible tandem PSCs integrated with commercially available solar technology on flexible substrates could be a good choice for practical application.

Declaration of Competing Interest

The authors declare that they have no known competing financial interests or personal relationships that could have appeared to influence the work reported in this paper.

Acknowledgements

This work was supported by the Research Grants Council (RGC) of Hong Kong, China (Project No. 15210319).

References

- [1] M.A. Green, A. Ho-Baillie, H.J. Snaith, The emergence of perovskite solar cells, *Nat. Photon* 8 (2014) 506–514.
- [2] H.-S. Kim, C.-R. Lee, J.-H. Im, K.-B. Lee, T. Moehl, A. Marchioro, S.-J. Moon, R. Humphry-Baker, J.-H. Yum, J.E. Moser, M. Grätzel, N.-G. Park, Lead iodide perovskite sensitized all-solid-state submicron thin film mesoscopic solar cell with efficiency exceeding 9, *Sci. Rep.* 2 (2012) 591.
- [3] H. Tan, A. Jain, O. Voznyy, X. Lan, F.P. García de Arquer, J.Z. Fan, R. Quintero-Bermudez, M. Yuan, B. Zhang, Y. Zhao, F. Fan, P. Li, L.N. Quan, Y. Zhao, Z.H. Lu, Z. Yang, S. Hoogland, E.H. Sargent, Efficient and stable solution-processed planar perovskite solar cells via contact passivation, *Science* 355 (2017) 722–726.
- [4] A. Kojima, K. Teshima, Y. Shirai, T. Miyasaka, Organometal halide perovskites as visible-light sensitizers for photovoltaic cells, *J. Am. Chem. Soc.* 131 (2009) 6050–6051.
- [5] M. Grätzel, The rise of highly efficient and stable perovskite solar cells, *Acc. Chem. Res.* 50 (2017) 487–491.
- [6] A.K. Jena, A. Kulkarni, T. Miyasaka, Halide perovskite photovoltaics: background, status, and future prospects, *Chem. Rev.* 119 (2019) 3036–3103.
- [7] Q. Tai, P. You, H. Sang, Z. Liu, C. Hu, H.L.W. Chan, F. Yan, Efficient and stable perovskite solar cells prepared in ambient air irrespective of the humidity, *Nat. Commun.* 7 (2016) 11105(Article).
- [8] Q. Tai, F. Yan, Emerging semitransparent solar cells: materials and device design, *Adv. Mater.* 29 (2017) 1700192(Article).
- [9] G. Tang, P. You, Q. Tai, R. Wu, F. Yan, Performance enhancement of perovskite solar cells induced by lead acetate as an additive, *Sol. RRL* 2 (2018) 1800066(Article).
- [10] G. Tang, P. You, Q. Tai, A. Yang, J. Cao, F. Zheng, Z. Zhou, J. Zhao, P.K.L. Chan, F. Yan, Solution-phase epitaxial growth of perovskite films on 2D material flakes for high-performance solar cells, *Adv. Mater.* 31 (2019) 1807689(Article).
- [11] Y. Zhao, K. Zhu, Organic-inorganic hybrid lead halide perovskites for optoelectronic and electronic applications, *Chem. Soc. Rev.* 45 (2016) 655–689.
- [12] S.D. Stranks, H.J. Snaith, Metal-halide perovskites for photovoltaic and light-emitting devices, *Nat. Nanotechnol.* 10 (2015) 391–402.
- [13] D. Kim, H.J. Jung, I.J. Park, B.W. Larson, S.P. Dunfield, C. Xiao, J. Kim, J. Tong, P. Boomgongkolras, S.G. Ji, F. Zhang, S.R. Pae, M. Kim, S.B. Kang, V. Dravid, J.J. Berry, J.Y. Kim, K. Zhu, D.H. Kim, B. Shin, Efficient, stable silicon tandem cells enabled by anion-engineered wide-bandgap perovskites, *Science* 368 (2020) 155–160.
- [14] National Renewable Energy Laboratory (NREL), Best Research-Cell Efficiencies, <https://www.nrel.gov/pv/assets/pdfs/best-research-cell-efficiencies.20200104.pdf>, Accessed January, 2021.
- [15] J.H. Heo, D.S. Lee, D.H. Shin, S.H. Im, Recent advancements in and perspectives on flexible hybrid perovskite solar cells, *J. Mater. Chem. A* 7 (2019) 888–900.
- [16] D. Yang, R. Yang, S. Priya, S. Liu, Recent advances in flexible perovskite solar cells: fabrication and applications, *Angew. Chem. Int. Ed.* 58 (2019) 4466–4483.
- [17] X. Meng, Z. Cai, Y. Zhang, X. Hu, Z. Xing, Z. Huang, Z. Huang, Y. Cui, T. Hu, M. Su, X. Liao, L. Zhang, F. Wang, Y. Song, Y. Chen, Bio-inspired vertebral design for scalable and flexible perovskite solar cells, *Nat. Commun.* 11 (2020) 3016(Article).
- [18] M. Kaltenbrunner, G. Adam, E.D. Głowacki, M. Drack, R. Schwödauer, L. Leonat, D.H. Apaydin, H. Groiss, M.C. Scharber, M.S. White, N.S. Sariciftci, S. Bauer, Flexible high power-per-weight perovskite solar cells with chromium oxide–metal contacts for improved stability in air, *Nat. Mater.* 14 (2015) 1032–1039.

- [19] K. Huang, K. Yang, H. Li, S. Zheng, J. Wang, H. Guo, Y. Peng, X. Zhong, J. Yang, γ -ray radiation on flexible perovskite solar cells, *ACS Appl. Energy Mater.* 3 (2020) 7318–7324.
- [20] L. Li, S. Zhang, Z. Yang, E.E.S. Berthold, W. Chen, Recent advances of flexible perovskite solar cells, *J. Energy Chem.* 27 (2018) 673–689.
- [21] X. Hu, Z. Huang, F. Li, M. Su, Z. Huang, Z. Zhao, Z. Cai, X. Yang, X. Meng, P. Li, Y. Wang, M. Li, Y. Chen, Y. Song, Nacre-inspired crystallization and elastic “brick-and-mortar” structure for a wearable perovskite solar module, *Energy Environ. Sci.* 12 (2019) 979–987.
- [22] L. Yang, M. Singh, S.-W. Shen, K.-Y. Chih, S.-W. Liu, C.-I. Wu, C.-W. Chu, H.-W. Lin, *Adv. Funct. Mater.* (2020) 2008259(Article).
- [23] S. Park, S.W. Heo, W. Lee, D. Inoue, Z. Jiang, K. Yu, H. Jinno, D. Hashizume, M. Sekino, T. Yokota, K. Fukuda, K. Tajima, T. Someya, Self-powered ultra-flexible electronics via nano-grating-patterned organic photovoltaics, *Nature* 561 (2018) 516–521.
- [24] C. Li, S. Cong, Z. Tian, Y. Song, L. Yu, C. Lu, Y. Shao, J. Li, G. Zou, M.H. Rümmeli, S. Dou, J. Sun, Z. Liu, Flexible perovskite solar cell-driven photo-rechargeable lithium-ion capacitor for self-powered wearable strain sensors, *Nano Energy* 60 (2019) 247–256.
- [25] M.H. Kumar, N. Yantara, S. Dharani, M. Graetzel, S. Mhaisalkar, P.P. Boix, N. Mathews, Flexible, low-temperature, solution processed ZnO-based perovskite solid state solar cells, *Chem. Commun.* 49 (2013) 11089–11091.
- [26] P. Docampo, J.M. Ball, M. Darwich, G.E. Eperon, H.J. Snaith, Efficient organometal trihalide perovskite planar-heterojunction solar cells on flexible polymer substrates, *Nat. Commun.* 4 (2013) 2761(Article).
- [27] D. Liu, T.L. Kelly, Perovskite solar cells with a planar heterojunction structure prepared using room-temperature solution processing techniques, *Nat. Photon.* 8 (2014) 133–138.
- [28] B.J. Kim, D.H. Kim, Y.-Y. Lee, H.-W. Shin, G.S. Han, J.S. Hong, K. Mahmood, T.K. Ahn, Y.-C. Joo, K.S. Hong, N.-G. Park, S. Lee, H.S. Jung, Highly efficient and bending durable perovskite solar cells: toward a wearable power source, *Energy Environ. Sci.* 8 (2015) 916–921.
- [29] S.S. Shin, W.S. Yang, J.H. Noh, J.H. Suk, N.J. Jeon, J.H. Park, J.S. Kim, W.M. Seong, S.I. Seok, High-performance flexible perovskite solar cells exploiting Zn₂SnO₄ prepared in solution below 100 °C, *Nat. Commun.* 6 (2015) 7410(Article).
- [30] J. Yoon, H. Sung, G. Lee, W. Cho, N. Ahn, H.S. Jung, M. Choi, Superflexible, high-efficiency perovskite solar cells utilizing graphene electrodes: towards future foldable power sources, *Energy Environ. Sci.* 10 (2017) 337–345.
- [31] J. Feng, X. Zhu, Z. Yang, X. Zhang, J. Niu, Z. Wang, S. Zuo, S. Priya, S. Liu, D. Yang, Record efficiency stable flexible perovskite solar cell using effective additive assistant strategy, *Adv. Mater.* 30 (2018) 1801418(Article).
- [32] C. Wu, D. Wang, Y. Zhang, F. Gu, G. Liu, N. Zhu, W. Luo, D. Han, X. Guo, B. Qu, S. Wang, Z. Bian, Z. Chen, L. Xiao, FAPbI₃flexible solar cells with a record efficiency of 19.38% fabricated in air via ligand and additive synergistic process, *Adv. Funct. Mater.* 29 (2019) 1902974(Article).
- [33] L. Yang, Q. Xiong, Y. Li, P. Gao, B. Xu, H. Lin, X. Li, T. Miyasaka, Artemisinin-passivated mixed-cation perovskite films for durable flexible perovskite solar cells with over 21% efficiency, *J. Mater. Chem. A* 9 (2021) 1574–1582.
- [34] C. Roldán-Carmona, O. Malinkiewicz, A. Soriano, G. Mínguez Espallargas, A. García, P. Reinecke, T. Kroyer, M.I. Dar, M.K. Nazeeruddin, H.J. Bolink, Flexible high efficiency perovskite solar cells, *Energy Environ. Sci.* 7 (2014) 994–997.
- [35] K. Huang, Y. Peng, Y. Gao, J. Shi, H. Li, X. Mo, H. Huang, Y. Gao, L. Ding, J. Yang, High-performance flexible perovskite solar cells via precise control of electron transport layer, *Adv. Energy Mater.* 9 (2019) 1901419(Article).
- [36] M. Park, H.J. Kim, I. Jeong, J. Lee, H. Lee, H.J. Son, D.-E. Kim, M.J. Ko, Mechanically recoverable and highly efficient perovskite solar cells: investigation of intrinsic flexibility of organic-inorganic perovskite, *Adv. Energy Mater.* 5 (2015) 1501406(Article).
- [37] N.-G. Park, K. Zhu, Scalable fabrication and coating methods for perovskite solar cells and solar modules, *Nat. Rev. Mater.* 5 (2020) 333–350.
- [38] Z. Li, T.R. Klein, D.H. Kim, M. Yang, J.J. Berry, M.F.A.M. van Hest, K. Zhu, Scalable fabrication of perovskite solar cells, *Nat. Rev. Mater.* 3 (2018) 18017(Article).
- [39] Y. Galagan, F. Di Giacomo, H. Gorter, G. Kirchner, I. de Vries, R. Andriessen, P. Groen, Roll-to-roll slot die coated perovskite for efficient flexible solar cells, *Adv. Energy Mater.* 8 (2018) 1801935(Article).
- [40] T. Bu, J. Li, F. Zheng, W. Chen, X. Wen, Z. Ku, Y. Peng, J. Zhong, Y.-B. Cheng, F. Huang, Universal passivation strategy to slot-die printed SnO₂ for hysteresis-free efficient flexible perovskite solar module, *Nat. Commun.* 9 (2018) 4609(Article).
- [41] C. Bi, B. Chen, H. Wei, S. DeLuca, J. Huang, Efficient flexible solar cell based on composition-tailored hybrid perovskite, *Adv. Mater.* 29 (2017) 1605900(Article).
- [42] V. Zardetto, T.M. Brown, A. Reale, A. Di Carlo, Substrates for flexible electronics: a practical investigation on the electrical, film flexibility, optical, temperature, and solvent resistance properties, *J. Polym. Sci. B Polym. Phys.* 49 (2011) 638–648.
- [43] J. Chung, S.S. Shin, K. Hwang, G. Kim, K.W. Kim, D.S. Lee, W. Kim, B.S. Ma, Y.-K. Kim, T.-S. Kim, J. Seo, Record-efficiency flexible perovskite solar cell and module enabled by a porous-planar structure as an electron transport layer, *Energy Environ. Sci.* 13 (2020) 4854–4861.
- [44] P. Zeng, W. Deng, M. Liu, Recent advances of device components toward efficient flexible perovskite solar cells, *Sol. RRL* 4 (2020) 1900485(Article).
- [45] H. Xie, X. Yin, Y. Guo, J. Liu, W. Que, G. Wang, Recent progress of flexible perovskite solar cells, *Phys. Status Solidi RRL* 13 (2019) 1800566(Article).
- [46] M.M. Tavakoli, K.-H. Tsui, Q. Zhang, J. He, Y. Yao, D. Li, Z. Fan, Highly efficient flexible perovskite solar cells with antireflection and self-cleaning nanosstructures, *ACS Nano* 9 (2015) 10287–10295.
- [47] X. Dai, Y. Deng, C.H. Van Brackle, S. Chen, P.N. Rudd, X. Xiao, Y. Lin, B. Chen, Scalable fabrication of efficient perovskite solar modules on flexible glass substrates, *Adv. Energy Mater.* 10 (2020) 1903108(Article).
- [48] M. Li, Y.-G. Yang, Z.-K. Wang, T. Kang, Q. Wang, S.-H. Turren-Cruz, X.-Y. Gao, C.-S. Hsu, L.-S. Liao, A. Abate, Perovskite grains embraced in a soft fullerene network make highly efficient flexible solar cells with superior mechanical stability, *Adv. Mater.* 31 (2019) 1901519(Article).
- [49] G. Lee, M.-c Kim, Y.W. Choi, N. Ahn, J. Jang, J. Yoon, S.M. Kim, J.-G. Lee, D. Kang, H.S. Jung, M. Choi, Ultra-flexible perovskite solar cells with crumpling durability: toward a wearable power source, *Energy Environ. Sci.* 12 (2019) 3182–3191.
- [50] X. Hu, X. Meng, X. Yang, Z. Huang, Z. Xing, P. Li, L. Tan, M. Su, F. Li, Y. Chen, Y. Song, *Sci. Bull.* (2020) (doi.org/10.1016/j.scib.2020.10.023).
- [51] M. Li, W.-W. Zuo, A.G. Ricciardulli, Y.-G. Yang, Y.-H. Liu, Q. Wang, K.-L. Wang, G.-X. Li, M. Saliba, D. Di Girolamo, A. Abate, Z.-K. Wang, Embedded nickel-mesh transparent electrodes for highly efficient and mechanically stable flexible perovskite photovoltaics: toward a portable mobile energy source, *Adv. Mater.* 32 (2020) 2003422(Article).
- [52] Y.Y. Kim, T.-Y. Yang, R. Suhonen, A. Kemppainen, K. Hwang, N.J. Jeon, J. Seo, Roll-to-roll gravure-printed flexible perovskite solar cells using eco-friendly anti-solvent bathing with wide processing window, *Nat. Commun.* 11 (11) (2020) 5146(Article).
- [53] J.H. Heo, D.H. Shin, M.H. Jang, M.L. Lee, M.G. Kang, S.H. Im, Highly flexible, high-performance perovskite solar cells with adhesion promoted AuCl₃-doped graphene electrodes, *J. Mater. Chem. A* 5 (2017) 21146–21152.
- [54] Z.K. Liu, P. You, C. Xie, G.Q. Tang, F. Yan, Ultrathin and flexible perovskite solar cells with graphene transparent electrodes, *Nano Energy* 28 (2016) 151–157.
- [55] V. Babu, R. Fuentes Pineda, T. Ahmad, A.O. Alvarez, L.A. Castriotta, A. Di Carlo, F. Fabregat-Santiago, K. Wojciechowski, Improved stability of inverted and flexible perovskite solar cells with carbon electrode, *ACS Appl. Energy Mater.* 3 (2020) 5126–5134.
- [56] X. Xu, H. Wang, J. Wang, M. Muhammad, Z. Wang, P. Chen, W. Zhao, B. Kang, J. Zhang, C. Li, Y. Duan, Surface functionalization of a graphene cathode to facilitate ALD growth of an electron transport layer and realize high-performance flexible perovskite solar cells, *ACS Appl. Energy Mater.* 3 (2020) 4208–4216.
- [57] C. Wu, D. Wang, Y. Zhang, F. Gu, G. Liu, N. Zhu, W. Luo, D. Han, X. Guo, B. Qu, S. Wang, Z. Bian, Z. Chen, L. Xiao, FAPbI₃flexible solar cells with a record efficiency of 19.38% fabricated in air via ligand and additive synergistic process, *Adv. Funct. Mater.* 29 (2019) 1902974(Article).
- [58] W. Deng, F. Li, J. Li, M. Wang, Y. Hu, M. Liu, Anti-solvent free fabrication of FA-Based perovskite at low temperature towards to high performance flexible perovskite solar cells, *Nano Energy* 70 (2020) 104505(Article).
- [59] C. Ge, Z. Yang, X. Liu, Y. Song, A. Wang, Q. Dong, Stable and highly flexible perovskite solar cells with power conversion efficiency approaching 20% by elastic grain boundary encapsulation, *CCS Chem.* 2 (2020) 2035–2044.
- [60] J.-I. Park, J.H. Heo, S.-H. Park, K.I. Hong, H.G. Jeong, S.H. Im, H.-K. Kim, Highly flexible InSnO electrodes on thin colourless polyimide substrate for high-performance flexible CH₃NH₃PbI₃ perovskite solar cells, *J. Power Sources* 341 (2017) 340–347.
- [61] J. Song, X. Xu, J. Wu, Z. Lan, Low-temperature solution-processing high quality Nb-doped SnO₂nanocrystals-based electron transport layers for efficient planar perovskite solar cells, *Funct. Mater. Lett.* 12 (12) (2019) 1850091(Article).
- [62] G. Jeong, D. Koo, J. Seo, S. Jung, Y. Choi, J. Lee, H. Park, Suppressed interdiffusion and degradation in flexible and transparent metal electrode-based perovskite solar cells with a graphene interlayer, *Nano Lett.* 20 (2020) 3718–3727.
- [63] X. Meng, Z. Xing, X. Hu, Z. Huang, T. Hu, L. Tan, F. Li, Y. Chen, Stretchable perovskite solar cells with recoverable performance, *Angew. Chem. Int. Ed.* 59 (2020) 16602–16608.
- [64] M. Lee, Y. Jo, D.S. Kim, Y. Jun, Flexible organo-metal halide perovskite solar cells on a Ti metal substrate, *J. Mater. Chem. A* 3 (2015) 4129–4133.
- [65] M. Lee, Y. Jo, D.S. Kim, H.Y. Jeong, Y. Jun, Efficient, durable and flexible perovskite photovoltaic devices with Ag-embedded ITO as the top electrode on a metal substrate, *J. Mater. Chem. A* 3 (2015) 14592–14597.
- [66] J. Troughton, D. Bryant, K. Wojciechowski, M.J. Carnie, H. Snaith, D.A. Worsley, T.M. Watson, Highly efficient, flexible, indium-free perovskite solar cells employing metallic substrates, *J. Mater. Chem. A* 3 (2015) 9141–9145.
- [67] G.S. Han, S. Lee, M.L. Duff, F. Qin, J.-K. Lee, Highly bendable flexible perovskite solar cells on a nanoscale surface oxide layer of titanium metal plates, *ACS Appl. Mater. Interfaces* 10 (2018) 4697–4704.
- [68] J.H. Heo, D.H. Shin, M.L. Lee, M.G. Kang, S.H. Im, Efficient organic–inorganic hybrid flexible perovskite solar cells prepared by lamination of poly-triarylamine/CH₃NH₃PbI₃/anodized Ti metal substrate and graphene/PDMS transparent electrode substrate, *ACS Appl. Mater. Interfaces* 10 (2018) 31413–31421.
- [69] B. Abdollahi Nejand, P. Nazari, S. Gharibzadeh, V. Ahmadi, A. Moshaii, All-inorganic large-area low-cost and durable flexible perovskite solar cells using copper foil as a substrate, *Chem. Commun.* 53 (2017) 747–750.
- [70] H. Li, X. Li, W. Wang, J. Huang, J. Li, Y. Lu, J. Chang, J. Fang, W. Song, Highly foldable and efficient paper-based perovskite solar cells, *Sol. RRL* 3 (2019) 1800317(Article).
- [71] L. Gao, L. Chao, M. Hou, J. Liang, Y. Chen, H.-D. Yu, W. Huang, Flexible, transparent nanocellulose paper-based perovskite solar cells, *npj Flex. Electron.* 3 (2019) 4(Article).
- [72] K. Zhu, Z. Lu, S. Cong, G. Cheng, P. Ma, Y. Lou, J. Ding, N. Yuan, M.H. Rümmeli, G. Zou, *Sol. RRL* 15 (2019) 1902878(Article).
- [73] B. Dou, E.M. Miller, J.A. Christians, E.M. Sanehira, T.R. Klein, F.S. Barnes, S.E. Shaheen, S.M. Garner, S. Ghosh, A. Mallick, D. Basak, M.F.A.M. van Hest,

- High-performance flexible perovskite solar cells on ultrathin glass: implications of the TCO, *J. Phys. Chem. Lett.* 8 (2017) 4960–4966.
- [74] H.S. Jung, G.S. Han, N.-G. Park, M.J. Ko, Flexible perovskite solar cells, *Joule* 3 (2019) 1850–1880.
- [75] J.S. Lewis, M.S. Weaver, Thin-film permeation-barrier technology for flexible organic light-emitting devices, *IEEE J. Sel. Top. Quantum Electron.* 10 (2004) 45–57.
- [76] Z. Suo, E.Y. Ma, H. Gleskova, S. Wagner, Mechanics of rollable and foldable film-on-foil electronics, *Appl. Phys. Lett.* 74 (1999) 1177–1179.
- [77] A. Gerthoffer, C. Poulain, F. Roux, F. Emieux, L. Grenet, S. Perraud, CIGS solar cells on ultra-thin glass substrates: determination of mechanical properties by nanoindentation and application to bending-induced strain calculation, *Sol. Energy Mater. Sol. Cells* 166 (2017) 254–261.
- [78] H. Li, X. Li, W. Wang, J. Huang, J. Li, S. Huang, B. Fan, J. Fang, W. Song, Ultraflexible and biodegradable perovskite solar cells utilizing ultrathin cellophane paper substrates and TiO₂/Ag/TiO₂ transparent electrodes, *Sol. Energy* 188 (2019) 158–163.
- [79] H. Kim, C.M. Gilmore, A. Piqué, J.S. Horwitz, H. Mattoossi, H. Murata, Z.H. Kafafi, D.B. Chrisey, Electrical, optical, and structural properties of indium-tin-oxide thin films for organic light-emitting devices, *J. Appl. Phys.* 86 (1999) 6451–6461.
- [80] L. Yang, Y. Li, L. Wang, Y. Pei, Z. Wang, Y. Zhang, H. Lin, X. Li, Exfoliated fluorographene quantum dots as outstanding passivants for improved flexible perovskite solar cells, *ACS Appl. Mater. Interfaces* 12 (2020) 22992–23001.
- [81] J. Ahn, H. Hwang, S. Jeong, J. Moon, Metal-nanowire-electrode-based perovskite solar cells: challenging issues and new opportunities, *Adv. Energy Mater.* 7 (2017) 1602751(Article).
- [82] P. Zhang, I. Wyman, J. Hu, S. Lin, Z. Zhong, Y. Tu, Z. Huang, Y. Wei, Silver nanowires: synthesis technologies, growth mechanism and multifunctional applications, *Mater. Sci. Eng. B* 223 (2017) 1–23.
- [83] W. Cao, J. Li, H. Chen, J. Xue, Transparent electrodes for organic optoelectronic devices: a review, *J. Photon. Energy* 4 (2014) 040990(Article).
- [84] M. Lagrange, D.P. Langley, G. Giusti, C. Jiménez, Y. Bréchet, D. Bellet, Optimization of silver nanowire-based transparent electrodes: effects of density, size and thermal annealing, *Nanoscale* 7 (2015) 17410–17423.
- [85] T. Sannicolo, M. Lagrange, A. Cabos, C. Celle, J.-P. Simonato, D. Bellet, Metallic nanowire-based transparent electrodes for next generation flexible devices: a review, *Small* 12 (2016) 6052–6075.
- [86] C.F. Guo, Z. Ren, Flexible transparent conductors based on metal nanowire networks, *Mater. Today* 18 (2015) 143–154.
- [87] A. Kim, H. Lee, H.-C. Kwon, H.S. Jung, N.-G. Park, S. Jeong, Fully solution-processed transparent electrodes based on silver nanowire composites for perovskite solar cells, *Nanoscale* 8 (2016) 6308–6316.
- [88] H. Lu, J. Sun, H. Zhang, S. Lu, W.C.H. Choy, Room-temperature solution-processed and metal oxide-free nano-composite for the flexible transparent bottom electrode of perovskite solar cells, *Nanoscale* 8 (2016) 5946–5953.
- [89] H.-G. Im, S. Jeong, J. Jin, J. Lee, D.-Y. Youn, W.-T. Koo, S.-B. Kang, H.-J. Kim, J. Jang, D. Lee, H.-K. Kim, I.-D. Kim, J.-Y. Lee, B.-S. Bae, Hybrid crystalline-ITO/metal nanowire mesh transparent electrodes and their application for highly flexible perovskite solar cells, *NPG Asia Mater.* 8 (2016) e282e282–e282.
- [90] E. Lee, J. Ahn, H.-C. Kwon, S. Ma, K. Kim, S. Yun, All-solution-processed silver nanowire window electrode-based flexible perovskite solar cells enabled with amorphous metal oxide protection, *Adv. Energy Mater.* 8 (2018) 1702182(Article).
- [91] H. Yang, H.-C. Kwon, S. Ma, K. Kim, S.-C. Yun, G. Jang, J. Park, H. Lee, S. Goh, J. Moon, Energy level-graded Al-doped ZnO protection layers for copper nanowire-based window electrodes for efficient flexible perovskite solar cells, *ACS Appl. Mater. Interfaces* 12 (2020) 13824–13835.
- [92] K.K. Sears, M. Fievez, M. Gao, H.C. Weerasinghe, C.D. Easton, D. Vak, ITO-free flexible perovskite solar cells based on roll-to-roll, slot-die coated silver nanowire electrodes, *Sol. RRL* 1 (2017) 1700059(Article).
- [93] S. Kang, J. Jeong, S. Cho, Y.J. Yoon, S. Park, S. Lim, J.Y. Kim, H. Ko, Ultrathin, lightweight and flexible perovskite solar cells with an excellent power-per-weight performance, *J. Mater. Chem. A* 7 (2019) 1107–1114.
- [94] Y. Li, L. Meng, Y. Yang, G. Xu, Z. Hong, Q. Chen, J. You, G. Li, Y. Yang, Y. Li, High-efficiency robust perovskite solar cells on ultrathin flexible substrates, *Nat. Commun.* 7 (2016) 10214(Article).
- [95] P. Li, Z. Wu, H. Hu, Y. Zhang, T. Xiao, X. Lu, Z. Ren, G. Li, Z. Wu, J. Hao, H.-I Zhang, Z. Zheng, Efficient flexible perovskite solar cells using low-cost Cu top and bottom electrodes, *ACS Appl. Mater. Interfaces* 12 (2020) 26050–26059.
- [96] Z. Liu, J. Li, Z.-H. Sun, G. Tai, S.-P. Lau, F. Yan, The application of highly doped single-layer graphene as the top electrodes of semitransparent organic solar cells, *ACS Nano* 6 (2012) 810–818.
- [97] Z. Liu, J. Li, F. Yan, Package-free flexible organic solar cells with graphene top electrodes, *Adv. Mater.* 25 (2013) 4296–4301.
- [98] X. Meng, J. Zhou, J. Hou, X. Tao, S.H. Cheung, S.K. So, S. Yang, Versatility of carbon enables all carbon based perovskite solar cells to achieve high efficiency and high stability, *Adv. Mater.* 30 (2018) 1706975(Article).
- [99] S. Bae, H. Kim, Y. Lee, X. Xu, J.-S. Park, Y. Zheng, J. Balakrishnan, T. Lei, H. Ri Kim, Y.I. Song, Y.-J. Kim, K.S. Kim, B. Özylmaz, J.-H. Ahn, B.H. Hong, S. Iijima, Roll-to-roll production of 30-inch graphene films for transparent electrodes, *Nat. Nanotechnol.* 5 (2010) 574–578.
- [100] Z. Liu, P. You, C. Xie, G. Tang, F. Yan, Ultrathin and flexible perovskite solar cells with graphene transparent electrodes, *Nano Energy* 28 (2016) 151–157.
- [101] I. Jeon, T. Chiba, C. Delacou, Y. Guo, A. Kaskela, O. Reynaud, E.I. Kauppinen, S. Maruyama, Y. Matsuo, Single-walled carbon nanotube film as electrode in indium-free planar heterojunction perovskite solar cells: investigation of electron-blocking layers and dopants, *Nano Lett.* 15 (2015) 6665–6671.
- [102] I. Jeon, J. Yoon, N. Ahn, M. Atwa, C. Delacou, A. Anisimov, E.I. Kauppinen, M. Choi, S. Maruyama, Y. Matsuo, Carbon nanotubes versus graphene as flexible transparent electrodes in inverted perovskite solar cells, *J. Phys. Chem. Lett.* 8 (2017) 5395–5401.
- [103] Q. Luo, H. Ma, Q. Hou, Y. Li, J. Ren, X. Dai, Z. Yao, Y. Zhou, L. Xiang, H. Du, H. He, N. Wang, K. Jiang, H. Lin, H. Zhang, Z. Guo, All-carbon-electrode-based durable flexible perovskite solar cells, *Adv. Funct. Mater.* 28 (2018) 1706777.
- [104] E. Dauzon, Y. Lin, H. Faber, E. Yengel, X. Sallenave, C. Plesse, F. Goubard, A. Amassian, T.D. Anthopoulos, Stretchable and transparent conductive pedot:pss-based electrodes for organic photovoltaics and strain sensors applications, *Adv. Funct. Mater.* 30 (2020) 2001251(Article).
- [105] X. Fan, W. Nie, H. Tsai, N. Wang, H. Huang, Y. Cheng, R. Wen, L. Ma, F. Yan, Y. Xia, PEDOT:PSS for flexible and stretchable electronics: modifications, strategies, and applications, *Adv. Sci.* 6 (2019) 1900813(Article).
- [106] Y. Zhang, Z. Wu, P. Li, L.K. Ono, Y. Qi, J. Zhou, H. Shen, C. Surya, Z. Zheng, Fully solution-processed tco-free semitransparent perovskite solar cells for tandem and flexible applications, *Adv. Energy Mater.* 8 (2018) 1701569(Article).
- [107] X. Hu, X. Meng, L. Zhang, Y. Zhang, Z. Cai, Z. Huang, M. Su, Y. Wang, M. Li, F. Li, X. Yao, F. Wang, W. Ma, Y. Chen, Y. Song, A mechanically robust conducting polymer network electrode for efficient flexible perovskite solar cells, *Joule* 3 (2019) 2205–2218.
- [108] Q. Wang, C.-C. Chueh, M. Esfahani, A.K.Y. Jen, Modulation of PEDOT:PSS pH for efficient inverted perovskite solar cells with reduced potential loss and enhanced stability, *ACS Appl. Mater. Interfaces* 8 (2016) 32068–32076.
- [109] J. Jin, J. Li, Q. Tai, Y. Chen, D.D. Mishra, W. Deng, J. Xin, S. Guo, B. Xiao, X. Wang, Efficient and stable flexible perovskite solar cells based on graphene-AgNWs substrate and carbon electrode without hole transport materials, *J. Power Sources* 482 (2021) 228953(Article).
- [110] D.H. Jung, Y.J. Oh, Y.S. Nam, H. Lee, Effect of layer number on the properties of stable and flexible perovskite solar cells using two dimensional material, *J. Alloy. Compd.* 850 (2021) 156752(Article).
- [111] K. Mahmood, S. Sarwar, M.T. Mehran, Current status of electron transport layers in perovskite solar cells: materials and properties, *RSC Adv.* 7 (2017) 17044–17062.
- [112] C. Bi, Q. Wang, Y. Shao, Y. Yuan, Z. Xiao, J. Huang, Non-wetting surface-driven high-aspect-ratio crystalline grain growth for efficient hybrid perovskite solar cells, *Nat. Commun.* 6 (2015) 7747(Article).
- [113] S.S. Shin, W.S. Yang, J.H. Noh, J.H. Suk, N.J. Jeon, J.H. Park, J.S. Kim, W.M. Seong, S.I. Seok, High-performance flexible perovskite solar cells exploiting Zn2SnO4 prepared in solution below 100 °C, *Nat. Commun.* 6 (2015) 7410(Article).
- [114] S.S. Shin, W.S. Yang, E.J. Yeom, S.J. Lee, N.J. Jeon, Y.-C. Joo, I.J. Park, J.H. Noh, S.I. Seok, Tailoring of electron-collecting oxide nanoparticulate layer for flexible perovskite solar cells, *J. Phys. Chem. Lett.* 7 (2016) 1845–1851.
- [115] R. Azmi, C.-L. Lee, I.H. Jung, S.-Y. Jang, Simultaneous improvement in efficiency and stability of low-temperature-processed perovskite solar cells by interfacial control, *Adv. Energy Mater.* 8 (2018) 1702934(Article).
- [116] L. Zuo, Z. Gu, T. Ye, W. Fu, G. Wu, H. Li, H. Chen, Enhanced photovoltaic performance of CH3NH3PbI3perovskite solar cells through interfacial engineering using self-assembling monolayer, *J. Am. Chem. Soc.* 137 (2015) 2674–2679.
- [117] T.-Y. Jin, W. Li, Y.-Q. Li, Y.-X. Luo, Y. Shen, L.-P. Cheng, J.-X. Tang, High-performance flexible perovskite solar cells enabled by low-temperature ALD-assisted surface passivation, *Adv. Opt. Mater.* 6 (2018) 1801153(Article).
- [118] D. Yang, R. Yang, J. Zhang, Z. Yang, S. Liu, C. Li, High efficiency flexible perovskite solar cells using superior low temperature TiO₂, *Energy Environ. Sci.* 8 (2015) 3208–3214.
- [119] W. Qiu, U.W. Paetzold, R. Gehlhaar, V. Smirnov, H.-G. Boyen, J.G. Tait, B. Conings, W. Zhang, C.B. Nielsen, I. McCulloch, L. Froyen, P. Heremans, D. Cheyns, An electron beam evaporated TiO₂layer for high efficiency planar perovskite solar cells on flexible polyethylene terephthalate substrates, *J. Mater. Chem. A* 3 (2015) 22824–22829.
- [120] F. Di Giacomo, V. Zardetto, A. D'Epifanio, S. Pescetelli, F. Matteocci, S. Razza, A. Di Carlo, S. Licoccia, W.M.M. Kessels, M. Creatore, T.M. Brown, Flexible perovskite photovoltaic modules and solar cells based on atomic layer deposited compact layers and UV-irradiated TiO₂scaffolds on plastic substrates, *Adv. Energy Mater.* 5 (2015) 14101808(Article).
- [121] H.J. Snaith, A. Abate, J.M. Ball, G.E. Eperon, T. Leijtens, N.K. Noel, S.D. Stranks, J.T.-W. Wang, K. Wojciechowski, W. Zhang, Anomalous hysteresis in perovskite solar cells, *J. Phys. Chem. Lett.* 5 (2014) 1511–1515.
- [122] B. Chen, M. Yang, S. Priya, K. Zhu, Origin of -Vhysteresis in perovskite solar cells, *J. Phys. Chem. Lett.* 7 (2016) 905–917.
- [123] N. Ahn, K. Kwak, M.S. Jang, H. Yoon, B.Y. Lee, J.-K. Lee, P.V. Pikhitsa, J. Byun, M. Choi, Trapped charge-driven degradation of perovskite solar cells, *Nat. Commun.* 7 (2016) 13422(Article).
- [124] P. Qin, S. Tanaka, S. Ito, N. Tetreault, K. Manabe, H. Nishino, M.K. Nazeeruddin, M. Grätzel, Inorganic hole conductor-based lead halide perovskite solar cells with 12.4% conversion efficiency, *Nat. Commun.* 5 (2014) 3834(Article).
- [125] B.J. Kim, M.-c Kim, D.G. Lee, G. Lee, G.J. Bang, J.B. Jeon, M. Choi, H.S. Jung, Interface design of hybrid electron extraction layer for relieving hysteresis and retarding charge recombination in perovskite solar cells, *Adv. Mater. Interfaces* 5 (2018) 1800993(Article).
- [126] Y.-Q. Zhou, B.-S. Wu, G.-H. Lin, Z. Xing, S.-H. Li, L.-L. Deng, D.-C. Chen, D.-Q. Yun, S.-Y. Xie, Interfacing pristine C60onto TiO2for viable flexibility in perovskite solar cells by a low-temperature all-solution process, *Adv. Energy Mater.* 8 (2018) 1800399(Article).

- [127] J. Nam, J.H. Kim, C.S. Kim, J.-D. Kwon, S. Jo, Surface engineering of low-temperature processed mesoporous TiO₂via oxygen plasma for flexible perovskite solar cells, *ACS Appl. Mater. Interfaces* 12 (2020) 12648–12655.
- [128] Q. Jiang, L. Zhang, H. Wang, X. Yang, J. Meng, H. Liu, Z. Yin, J. Wu, X. Zhang, Enhanced electron extraction using SnO₂ for high-efficiency planar-structure HC(NH₂)₂PbI₃-based perovskite solar cells, *Nat. Energy* 2 (2016) 16177(Article).
- [129] M. Park, J.-Y. Kim, H.J. Son, C.-H. Lee, S.S. Jang, M.J. Ko, Low-temperature solution-processed Li-doped SnO₂ as an effective electron transporting layer for high-performance flexible and wearable perovskite solar cells, *Nano Energy* 26 (2016) 208–215.
- [130] C. Wang, L. Guan, D. Zhao, Y. Yu, C.R. Grice, Z. Song, R.A. Awni, J. Chen, J. Wang, X. Zhao, Y. Yan, Water vapor treatment of low-temperature deposited SnO₂electron selective layers for efficient flexible perovskite solar cells, *ACS Energy Lett.* 2 (2017) 2118–2124.
- [131] C. Liu, L. Zhang, X. Zhou, J. Gao, W. Chen, X. Wang, B. Xu, Hydrothermally treated SnO₂as the electron transport layer in high-efficiency flexible perovskite solar cells with a certificated efficiency of 17.3, *Adv. Funct. Mater.* 29 (2019) 1807604(Article).
- [132] D. Yang, R. Yang, K. Wang, C. Wu, X. Zhu, J. Feng, X. Ren, G. Fang, S. Priya, S. Liu, High efficiency planar-type perovskite solar cells with negligible hysteresis using EDTA-complexed SnO₂, *Nat. Commun.* 9 (2018) 3239(Article).
- [133] A.S. Subbiah, N. Mathews, S. Mhaisalkar, S.K. Sarkar, Novel plasma-assisted low-temperature-processed SnO₂thin films for efficient flexible perovskite photovoltaics, *ACS Energy Lett.* 3 (2018) 1482–1491.
- [134] K. Huang, Y. Peng, Y. Gao, J. Shi, H. Li, X. Mo, H. Huang, Y. Gao, L. Ding, High-performance flexible perovskite solar cells via precise control of electron transport layer, *Adv. Energy Mater.* 9 (2019) 1901419(Article).
- [135] Q. Dong, J. Li, Y. Shi, M. Chen, L.K. Ono, K. Zhou, C. Zhang, Y. Qi, Y. Zhou, N.P. Padture, L. Wang, Improved SnO₂electron transport layers solution-deposited at near room temperature for rigid or flexible perovskite solar cells with high efficiencies, *Adv. Energy Mater.* 9 (2019) 1900834(Article).
- [136] M. Zhong, Y. Liang, J. Zhang, Z. Wei, Q. Li, D. Xu, Highly efficient flexible MAPbI₃solar cells with a fullerene derivative-modified SnO₂layer as the electron transport layer, *J. Mater. Chem. A* 7 (2019) 6659–6664.
- [137] X. Liu, X. Yang, X. Liu, Y. Zhao, J. Chen, Y. Gu, High efficiency flexible perovskite solar cells using SnO₂/graphene electron selective layer and silver nanowires electrode, *Appl. Phys. Lett.* 113 (2018) 203903.
- [138] N. Zhu, X. Qi, Y. Zhang, G. Liu, C. Wu, D. Wang, X. Guo, W. Luo, X. Li, H. Hu, Z. Chen, L. Xiao, B. Qu, High efficiency (18.53%) of flexible perovskite solar cells via the insertion of potassium chloride between SnO₂and CH₃NH₃PbI₃layers, *ACS Appl. Energy Mater.* 2 (2019) 3676–3682.
- [139] D. Yang, R. Yang, X. Ren, X. Zhu, Z. Yang, C. Li, S. Liu, Hysteresis-suppressed high-efficiency flexible perovskite solar cells using solid-state ionic-liquids for effective electron transport, *Adv. Mater.* 28 (2016) 5206–5213.
- [140] U. Ryu, S. Jee, J.-S. Park, I.K. Han, J.H. Lee, M. Park, K.M. Choi, Nanocrystalline titanium metal–organic frameworks for highly efficient and flexible perovskite solar cells, *ACS Nano* 12 (2018) 4968–4975.
- [141] X. Zhao, L. Tian, T. Liu, H. Liu, S. Wang, X. Li, O. Fenwick, S. Lei, W. Hu, Room-temperature-processed fullerene single-crystalline nanoparticles for high-performance flexible perovskite photovoltaics, *J. Mater. Chem. A* 7 (2019) 1509–1518.
- [142] W. Chu, X. Li, S. Li, J. Hou, Q. Jiang, J. Yang, High-performance flexible perovskite solar cells with a metal sulfide electron transport layer of SnS₂by room-temperature vacuum deposition, *ACS Appl. Energy Mater.* 2 (2019) 382–388.
- [143] X. Xu, Q. Chen, Z. Hong, H. Zhou, Z. Liu, W.-H. Chang, P. Sun, H. Chen, N.D. Marco, M. Wang, Y. Yang, Working mechanism for flexible perovskite solar cells with simplified architecture, *Nano Lett.* 15 (2015) 6514–6520.
- [144] J.H. Heo, M.H. Lee, H.J. Han, B.R. Patil, J.S. Yu, S.H. Im, Highly efficient low temperature solution processable planar type CH₃NH₃PbI₃perovskite flexible solar cells, *J. Mater. Chem. A* 4 (2016) 1572–1578.
- [145] X. Liu, C.-C. Chueh, Z. Zhu, S.B. Jo, Y. Sun, A.K.Y. Jen, Highly crystalline Zn₂SnO₄nanoparticles as efficient electron-transporting layers toward stable inverted and flexible conventional perovskite solar cells, *J. Mater. Chem. A* 4 (2016) 15294–15301.
- [146] S.Y. Park, M.Y. Baek, Y. Ju, D.H. Kim, C.S. Moon, J.H. Noh, H.S. Jung, Simultaneous ligand exchange fabrication of flexible perovskite solar cells using newly synthesized uniform tin oxide quantum dots, *J. Phys. Chem. Lett.* 9 (2018) 5460–5467.
- [147] B. Cao, L. Yang, S. Jiang, H. Lin, N. Wang, X. Li, Flexible quintuple cation perovskite solar cells with high efficiency, *J. Mater. Chem. A* 7 (2019) 4960–4970.
- [148] H. Xie, X. Yin, Y. Guo, D. Liu, T. Liang, G. Wang, W. Que, Hole transport free flexible perovskite solar cells with cost-effective carbon electrodes, *Nanotechnology* 32 (2020) 105205(Article).
- [149] Y. Han, S. Meyer, Y. Dkhissi, K. Weber, J.M. Pringle, U. Bach, L. Spiccia, Y.-B. Cheng, Degradation observations of encapsulated planar CH₃NH₃PbI₃perovskite solar cells at high temperatures and humidity, *J. Mater. Chem. A* 3 (2015) 8139–8147.
- [150] I. Jeong, H. Jung, M. Park, J.S. Park, H.J. Son, J. Joo, J. Lee, M.J. Ko, A tailored TiO₂ electron selective layer for high-performance flexible perovskite solar cells via low temperature UV process, *Nano Energy* 28 (2016) 380–389.
- [151] C. Liu, M. Cai, Y. Yang, Z. Arain, Y. Ding, X. Shi, P. Shi, S. Ma, T. Hayat, A. Alsaedi, J. Wu, S. Dai, G. Cao, A C60/TiOxbilayer for conformal growth of perovskite films for UV stable perovskite solar cells, *J. Mater. Chem. A* 7 (2019) 11086–11094.
- [152] Z. Wu, P. Li, J. Zhao, T. Xiao, H. Hu, P. Sun, Z. Wu, J. Hao, C. Sun, H. Zhang, Z. Huang, Z. Zheng, Low-temperature-deposited TiO₂nanopillars for efficient and flexible perovskite solar cells, *Adv. Mater. Interfaces* 8 (2021) 2001512(Article).
- [153] J. You, L. Meng, T.-B. Song, T.-F. Guo, Y. Yang, W.-H. Chang, Z. Hong, H. Chen, H. Zhou, Q. Chen, Y. Liu, N. De Marco, Y. Yang, Improved air stability of perovskite solar cells via solution-processed metal oxide transport layers, *Nat. Nanotechnol.* 11 (2016) 75–81.
- [154] H. Zhang, J. Cheng, F. Lin, H. He, J. Mao, K.S. Wong, A.K.Y. Jen, W.C.H. Choy, Pinhole-free and surface-nanostructured NiOxFilm by room-temperature solution process for high-performance flexible perovskite solar cells with good stability and reproducibility, *ACS Nano* 10 (2016) 1503–1511.
- [155] X. Yin, P. Chen, M. Que, Y. Xing, W. Que, C. Niu, J. Shao, Highly efficient flexible perovskite solar cells using solution-derived NiOxhole contacts, *ACS Nano* 10 (2016) 3630–3636.
- [156] Q. He, K. Yao, X. Wang, X. Xia, S. Leng, F. Li, Room-temperature and solution-processable Cu-doped nickel oxide nanoparticles for efficient hole-transport layers of flexible large-area perovskite solar cells, *ACS Appl. Mater. Interfaces* 9 (2017) 41887–41897.
- [157] P. Ru, E. Bi, Y. Zhang, Y. Wang, W. Kong, Y. Sha, W. Tang, P. Zhang, Y. Wu, W. Chen, X. Yang, H. Chen, L. Han, High electron affinity enables fast hole extraction for efficient flexible inverted perovskite solar cells, *Adv. Energy Mater.* 10 (2020) 1903487(Article).
- [158] Z. Zhu, Y. Bai, T. Zhang, Z. Liu, X. Long, Z. Wei, Z. Wang, L. Zhang, J. Wang, F. Yan, S. Yang, *Angew. Chem. Int. Ed.* 53 (2014) 12571–12575.
- [159] C.-H. Hou, J.-J. Shyue, W.-F. Su, F.-Y. Tsai, Catalytic metal-induced crystallization of sol-gel metal oxides for high-efficiency flexible perovskite solar cells, *J. Mater. Chem. A* 6 (2018) 16450–16457.
- [160] S. Cong, G. Zou, Y. Lou, H. Yang, Y. Su, J. Zhao, C. Zhang, P. Ma, Z. Lu, H. Fan, Z. Huang, Fabrication of nickel oxide nanopillar arrays on flexible electrodes for highly efficient perovskite solar cells, *Nano Lett.* 19 (2019) 3676–3683.
- [161] J.W. Jo, M.-S. Seo, M. Park, J.-Y. Kim, J.S. Park, I.K. Han, H. Ahn, J.W. Jung, B.-H. Sohn, M.J. Ko, H.J. Son, Improving performance and stability of flexible planar-heterojunction perovskite solar cells using polymeric hole-transport material, *Adv. Funct. Mater.* 26 (2016) 4464–4471.
- [162] S.S. Reddy, S. Shin, U.K. Aryal, R. Nishikubo, A. Saeki, M. Song, S.-H. Jin, Highly efficient air-stable/hysteresis-free flexible inverted-type planar perovskite and organic solar cells employing a small molecular organic hole transporting material, *Nano Energy* 41 (2017) 10–17.
- [163] M. Najafi, F. Di Giacomo, D. Zhang, S. Shanmugam, A. Senes, W. Verhees, A. Hadipour, Y. Galagan, T. Aeroutsos, S. Veenstra, R. Andriessen, Highly efficient and stable flexible perovskite solar cells with metal oxides nanoparticle charge extraction layers, *Small* 14 (2018) 1702775(Article).
- [164] H.I. Kim, M.-J. Kim, K. Choi, C. Lim, Y.-H. Kim, S.-K. Kwon, T. Park, Improving the performance and stability of inverted planar flexible perovskite solar cells employing a novel NDI-based polymer as the electron transport layer, *Adv. Energy Mater.* 8 (2018) 1702872(Article).
- [165] X. Yu, Z. Li, X. Sun, C. Zhong, Z. Zhu, Za Li, A.K.Y. Jen, Dopant-free dicyanofluoranthene-based hole transporting material with low cost enables efficient flexible perovskite solar cells, *Nano Energy* 82 (2021) 105701(Article).
- [166] F. Yang, J. Liu, H.E. Lim, Y. Ishikura, K. Shinokita, Y. Miyachi, A. Wakamiya, Y. Murata, K. Matsuda, High bending durability of efficient flexible perovskite solar cells using metal oxide electron transport layer, *J. Phys. Chem. C* 122 (2018) 17088–17095.
- [167] H. Zhang, J. Cheng, F. Lin, H. He, J. Mao, K.S. Wong, A.K. Jen, W.C.H. Choy, Pinhole-free and surface-nanostructured NiOxFilm by room-temperature solution process for high-performance flexible perovskite solar cells with good stability and reproducibility, *ACS Nano* 10 (2016) 1503–1511.
- [168] D.B. Kim, J.W. Lee, Y.S. Cho, Anisotropic in situ strain-engineered halide perovskites for high mechanical flexibility, *Adv. Funct. Mater.* 31 (2021) 2007131(Article).
- [169] N. Rolston, B.L. Watson, C.D. Bailie, M.D. McGehee, J.P. Bastos, R. Gehlhaar, J.-E. Kim, D. Valk, A.T. Mallajosyula, G. Gupta, A.D. Mohite, R.H. Dauskardt, Mechanical integrity of solution-processed perovskite solar cells, *Extrem. Mech. Lett.* 9 (2016) 353–358.
- [170] H. Wang, C. Zhu, L. Liu, S. Ma, P. Liu, J. Wu, C. Shi, Q. Du, Y. Hao, S. Xiang, H. Chen, P. Chen, Y. Bai, H. Zhou, Y. Li, Q. Chen, Interfacial residual stress relaxation in perovskite solar cells with improved stability, *Adv. Mater.* 31 (2019) 1904408(Article).
- [171] Z. Huang, X. Hu, C. Liu, X. Meng, Z. Huang, J. Yang, X. Duan, J. Long, Z. Zhao, L. Tan, Y. Song, Y. Chen, Water-resistant and flexible perovskite solar cells via a glued interfacial layer, *Adv. Funct. Mater.* 29 (2019) 1902629(Article).
- [172] J.H. Yun, I. Lee, T.-S. Kim, M.J. Ko, J.Y. Kim, H.J. Son, Synergistic enhancement and mechanism study of mechanical and moisture stability of perovskite solar cells introducing polyethylene-imine into the CH₃NH₃PbI₃/HTM interface, *J. Mater. Chem. A* 3 (2015) 22176–22182.
- [173] X. Hu, Z. Huang, X. Zhou, P. Li, Y. Wang, Z. Huang, M. Su, W. Ren, F. Li, M. Li, Y. Chen, Y. Song, Wearable large-scale perovskite solar-power source via nanocellular scaffold, *Adv. Mater.* 29 (2017) 1703236(Article).
- [174] T. Jeon, H.M. Jin, S.H. Lee, J.M. Lee, H.I. Park, M.K. Kim, K.J. Lee, B. Shin, S.O. Kim, Laser crystallization of organic-inorganic hybrid perovskite solar cells, *ACS Nano* 10 (2016) 7907–7914.
- [175] P. You, G. Li, G. Tang, J. Cao, F. Yan, Ultrafast laser-annealing of perovskite films for efficient perovskite solar cells, *Energy Environ. Sci.* 13 (2020) 1187–1196.
- [176] T. Lei, F. Li, X. Zhu, H. Dong, Z. Niu, S. Ye, W. Zhao, J. Xi, B. Jiao, L. Ding, Z. Wu, Flexible perovskite solar modules with functional layers fully vacuum deposited, *Sol. RRL* 4 (2020) 2000292(Article).

- [177] Y. Hu, S. Zhang, T. Shu, T. Qiu, F. Bai, W. Ruan, F. Xu, Highly efficient flexible solar cells based on a room-temperature processed inorganic perovskite, *J. Mater. Chem. A* 6 (2018) 20365–20373.
- [178] H. Rao, S. Ye, F. Gu, Z. Zhao, Z. Liu, Z. Bian, C. Huang, Morphology controlling of all-inorganic perovskite at low temperature for efficient rigid and flexible solar cells, *Adv. Energy Mater.* 8 (2018) 1800758(Article).
- [179] J. Xi, Z. Wu, B. Jiao, H. Dong, C. Ran, C. Piao, T. Lei, T.-B. Song, W. Ke, T. Yokoyama, X. Hou, M.G. Kanatzidis, Multichannel interdiffusion driven FASnI_3 film formation using aqueous hybrid salt/polymer solutions toward flexible lead-free perovskite solar cells, *Adv. Mater.* 29 (2017) 1606964(Article).
- [180] Q. Tai, X. Guo, G. Tang, P. You, T.-W. Ng, D. Shen, J. Cao, C.-K. Liu, N. Wang, Y. Zhu, C.-S. Lee, F. Yan, Antioxidant grain passivation for air-stable tin-based perovskite solar cells, *Angew. Chem. Int. Ed.* 58 (2019) 806–810.
- [181] C. Bi, B. Chen, H. Wei, S. DeLuca, J. Huang, Efficient flexible solar cell based on composition-tailored hybrid perovskite, *Adv. Mater.* 29 (2017) 1605900(Article).
- [182] X. Yang, H. Yang, X. Hu, W. Li, Z. Fang, K. Zhang, R. Huang, J. Li, Z. Yang, Y. Song, Low-temperature interfacial engineering for flexible CsPbI_2Br perovskite solar cells with high performance beyond 15, *J. Mater. Chem. A* 8 (2020) 5308–5314.
- [183] M. Li, Y.-G. Yang, Z.-K. Wang, T. Kang, Q. Wang, S.-H. Turren-Cruz, X.-Y. Gao, C.-S. Hsu, L.-S. Liao, A. Abate, Perovskite grains embraced in a soft fullerene network make highly efficient flexible solar cells with superior mechanical stability, *Adv. Mater.* 31 (2019) 1901519(Article).
- [184] C. Liu, J. Sun, X.-F. Jiang, L. Huang, Q. Lou, Y.-B. Cheng, S. Song, Z. Ge, A universal tactic of using Lewis-base polymer-CNTs composites as additives for high performance cm²-sized and flexible perovskite solar cells, *Sci. China Chem.* 64 (2020) 281–292.
- [185] Y. Rong, Y. Hu, A. Mei, H. Tan, M.I. Saidaminov, S.I. Seok, M.D. McGehee, E.H. Sargent, H. Han, Challenges for commercializing perovskite solar cells, *Science* 361 (2018) eaat8235 (Article).
- [186] N.-G. Park, M. Grätzel, T. Miyasaka, K. Zhu, K. Emery, Towards stable and commercially available perovskite solar cells, *Nat. Energy* 1 (2016) 16152.
- [187] F. Di Giacomo, A. Fakharuddin, R. Jose, T.M. Brown, Progress, challenges and perspectives in flexible perovskite solar cells, *Energy Environ. Sci.* 9 (2016) 3007–3035.
- [188] Y. Deng, X. Zheng, Y. Bai, Q. Wang, J. Zhao, Surfactant-controlled ink drying enables high-speed deposition of perovskite films for efficient photovoltaic modules, *Nat. Energy* 3 (2018) 560–566.
- [189] Y. Deng, C.H. Van Brackle, X. Dai, J. Zhao, B. Chen, J. Huang, Tailoring solvent coordination for high-speed, room-temperature blading of perovskite photovoltaic films, *Sci. Adv.* 5 (2019) eaax7537 (Article).
- [190] T.M. Schmidt, T.T. Larsen-Olsen, J.E. Carlé, D. Angmo, F.C. Krebs, Upscaling of perovskite solar cells: fully ambient roll processing of flexible perovskite solar cells with printed back electrodes, *Adv. Energy Mater.* 5 (2015) 1500569(Article).
- [191] Y. Galagan, F. Di Giacomo, H. Gorter, G. Kirchner, I. de Vries, R. Andriessen, P. Groen, Roll-to-roll slot die coated perovskite for efficient flexible solar cells, *Adv. Energy Mater.* 8 (2018) 1801935(Article).
- [192] J.-E. Kim, S.-S. Kim, C. Zuo, M. Gao, D. Vak, D.-Y. Kim, Humidity-tolerant roll-to-roll fabrication of perovskite solar cells via polymer-additive-assisted hot slot die deposition, *Adv. Funct. Mater.* 29 (2019) 1809194(Article).
- [193] Z. Gu, L. Zuo, T.T. Larsen-Olsen, T. Ye, G. Wu, F.C. Krebs, H. Chen, Interfacial engineering of self-assembled monolayer modified semi-roll-to-roll planar heterojunction perovskite solar cells on flexible substrates, *J. Mater. Chem. A* 3 (2015) 24254–24260.
- [194] Z. Wang, L. Zeng, C. Zhang, Y. Lu, S. Qiu, C. Wang, C. Liu, L. Pan, S. Wu, J. Hu, G. Liang, P. Fan, H.-J. Egelhaaf, C.J. Brabec, F. Guo, Y. Mai, Rational interface design and morphology control for blade-coating efficient flexible perovskite solar cells with a record fill factor of 81, *Adv. Funct. Mater.* 30 (2020) 2001240(Article).
- [195] S. Das, B. Yang, G. Gu, P.C. Joshi, I.N. Ivanov, C.M. Rouleau, T. Ayutg, D.B. Geohegan, K. Xiao, High-performance flexible perovskite solar cells by using a combination of ultrasonic spray-coating and low thermal budget photonic curing, *ACS Photonics* 2 (2015) 680–686.
- [196] J. Li, Y. Liu, X. Ren, Z. Yang, R. Li, H. Su, X. Yang, J. Xu, H. Xu, J.-Y. Hu, A. Amassian, K. Zhao, S. Liu, Solution coating of superior large-area flexible perovskite thin films with controlled crystal packing, *Adv. Opt. Mater.* 5 (2017) 1700102(Article).
- [197] Z. Wei, H. Chen, K. Yan, S. Yang, Inkjet printing and instant chemical transformation of a $\text{CH}_3\text{NH}_3\text{PbI}_3$ /nanocarbon electrode and interface for planar perovskite solar cells, *Angew. Chem. Int. Ed.* 53 (2014) 13239–13243.
- [198] A.F. Palmstrom, G.E. Eperon, T. Leijtens, R. Prasanna, S.N. Habreutinger, W. Nemeth, E.A. Gaulding, S.P. Dunfield, M. Reese, S. Nanayakkara, T. Moot, J. Werner, J. Liu, B. To, S.T. Christensen, M.D. McGehee, M.F.A.M. van Hest, J.M. Luther, J.J. Berry, D.T. Moore, Enabling flexible all-perovskite tandem solar cells, *Joule* 3 (2019) 2193–2204.
- [199] Q. Fu, X. Tang, B. Huang, T. Hu, L. Tan, L. Chen, Y. Chen, Recent progress on the long-term stability of perovskite solar cells, *Adv. Sci.* 5 (2018) 1700387(Article).
- [200] H.C. Weerasinghe, Y. Dkhissi, A.D. Scully, R.A. Caruso, Y.-B. Cheng, Encapsulation for improving the lifetime of flexible perovskite solar cells, *Nano Energy* 18 (2015) 118–125.
- [201] E. Cho, Y.Y. Kim, D.S. Ham, J.H. Lee, J.-S. Park, J. Seo, S.-J. Lee, Highly efficient and stable flexible perovskite solar cells enabled by using plasma-polymerized-fluorocarbon antireflection layer, *Nano Energy* 82 (2021) 105737(Article).



Guanqi Tang is a Postdoctoral Fellow in Prof. Yan Feng's group in the Department of Applied Physics at Hong Kong Polytechnic University. Dr. Tang received his Ph.D. degree from Hong Kong Polytechnic University under supervision of Prof. YAN Feng. His research interests are organic-inorganic halide perovskite based electronic devices.



Feng Yan has research interests on organic electronics, 2D materials, solar cells, thin film transistors, biosensors and smart materials. He received his PhD degree in physics from Nanjing University in 1997 and then worked at the Department of Physics of Nanjing University as Associate Professor until Jan 2001. He joined the Engineering Department of Cambridge University in Feb 2001 as a Research Associate and joined National Physical Laboratory in UK in April 2006 as a Higher Research Scientist. He became an Assistant Professor at the Department of Applied Physics of the Hong Kong Polytechnic University in September 2006 and was promoted to Full Professor in 2016. He is a Fellow of Royal Society of Chemistry (FRSC) and a senior member of IEEE. He has published more than 200 papers in peer-reviewed journals, including *Adv. Mater.*, *Nature Commun.*, *Nano Lett.*, *JACS*, and given more than 70 invited talks in international conferences.